

Responses to Tomislav Hengl (Referee)

Summary comments

Comment 1: Section 2.2 needs to be extended. How was the sampling plan generated? Did you sample per soil horizon or at fixed depths? Did you take bulk samples or are the samples close-to-point support? Which laboratory methods you used and what is the average measurement error per texture fraction? These issues need to be clarified.

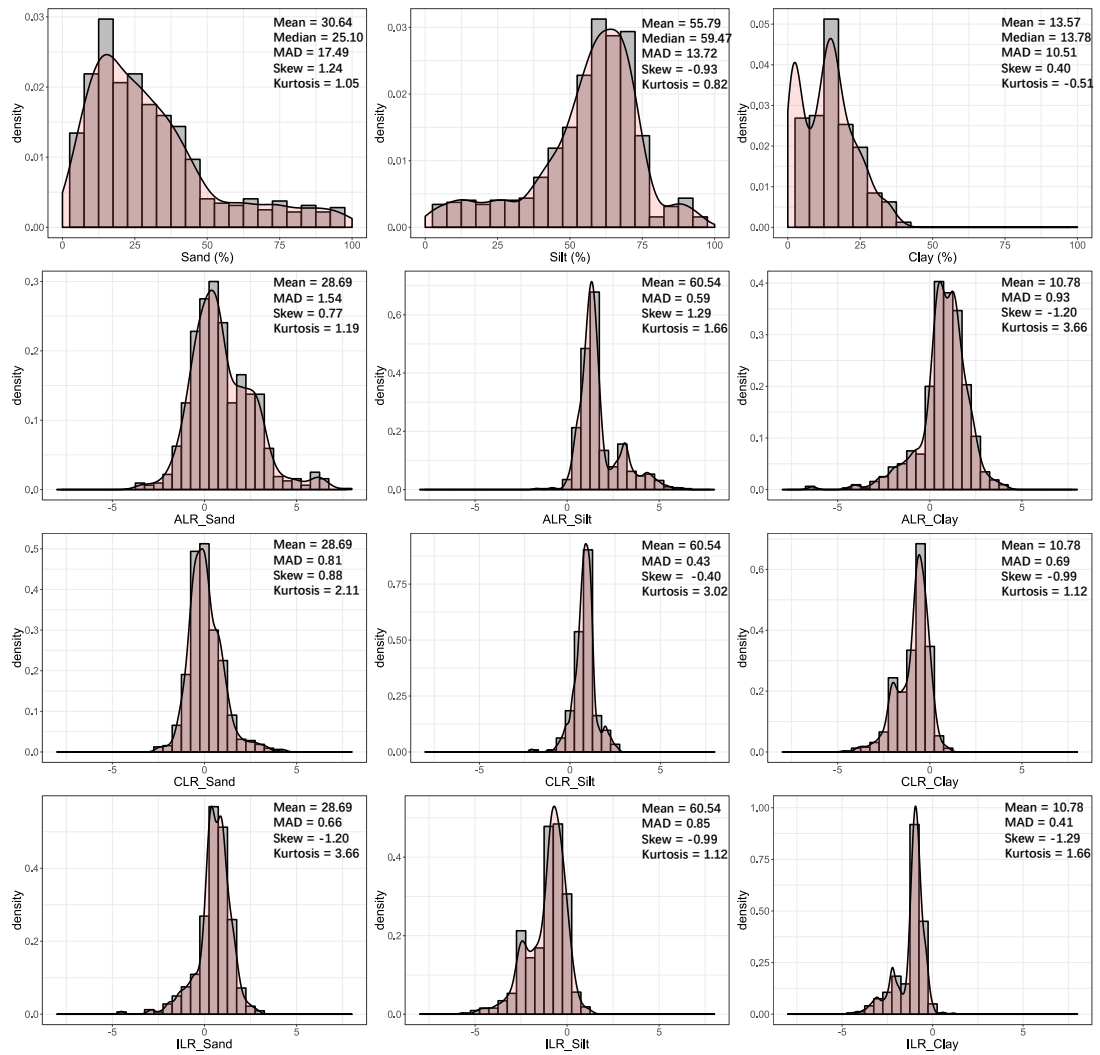
Response: Thanks for the referee's constructive comments, suggestions and questions, which can provide us encouragement to revise the paper to the best of our ability. We have added more details about soil samples such as the sampling strategy, sampling depth, sampling measurement, laboratory analysis methods and the average measurement error per texture fraction in our revised version.

P25L23: *"All soil samples had information about soil PSF (i.e., sand, silt and clay) using Malvern Mastersizer 2000 laser diffraction particle size analyzer (average measurement error is less than 3 %). The related environmental covariates were extracted using the extraction tool in ArcGIS, and the global position system (GPS) recorded the position information. Purposive sampling was used as the sampling strategy to collect soil samples and to characterize the spatial variability of soil PSF especially on such a regional scale of the study area (Zhu et al., 2008). In this strategy, sample sites were chosen based on the variability of soil formation factors, which represented the heterogeneity of the soil PSF in the HRB such as the distribution of climate and categorical maps we mentioned, etc. To reduce the noise effect of soil sample, the average of mixed 3–5 topsoil (0–20 cm) samples for each soil sample and its parallel sample was used as the final measurement. Subsequently, the samples were dried, analyzed and measurement of soil PSF (approximately 30 g of each sample). "*

Comment 2: Figures 2 (irregular scales of x-axis) and 8 (unreadable text and missing description of point colors) need to be improved following the comments I made in the text.

Response: Thanks for the referee's suggestions. We have modified figures 2 and 8 in our revised version. In figure 2, we put exactly the same scale (0-100% of sand, silt and clay and -8 to 8 of others for the x-axis), centered all ALR, CLR and ILR plots at 0, and removed "Min" and "Max" from the labels. In figure 8, we made the text size larger, explained the meaning of yellow points and green points, added right ratios to compare different performance, and removed the original data (a) and put it into Fig. 1.

Figure 2, P38L1:



“Figure 3. Descriptive statistical analysis for the original (untransformed) and log ratio transformed soil sampling data. Note that the means generated from log ratio transformed data were back-transformed to the real space.”

Figure 8, P50L1:

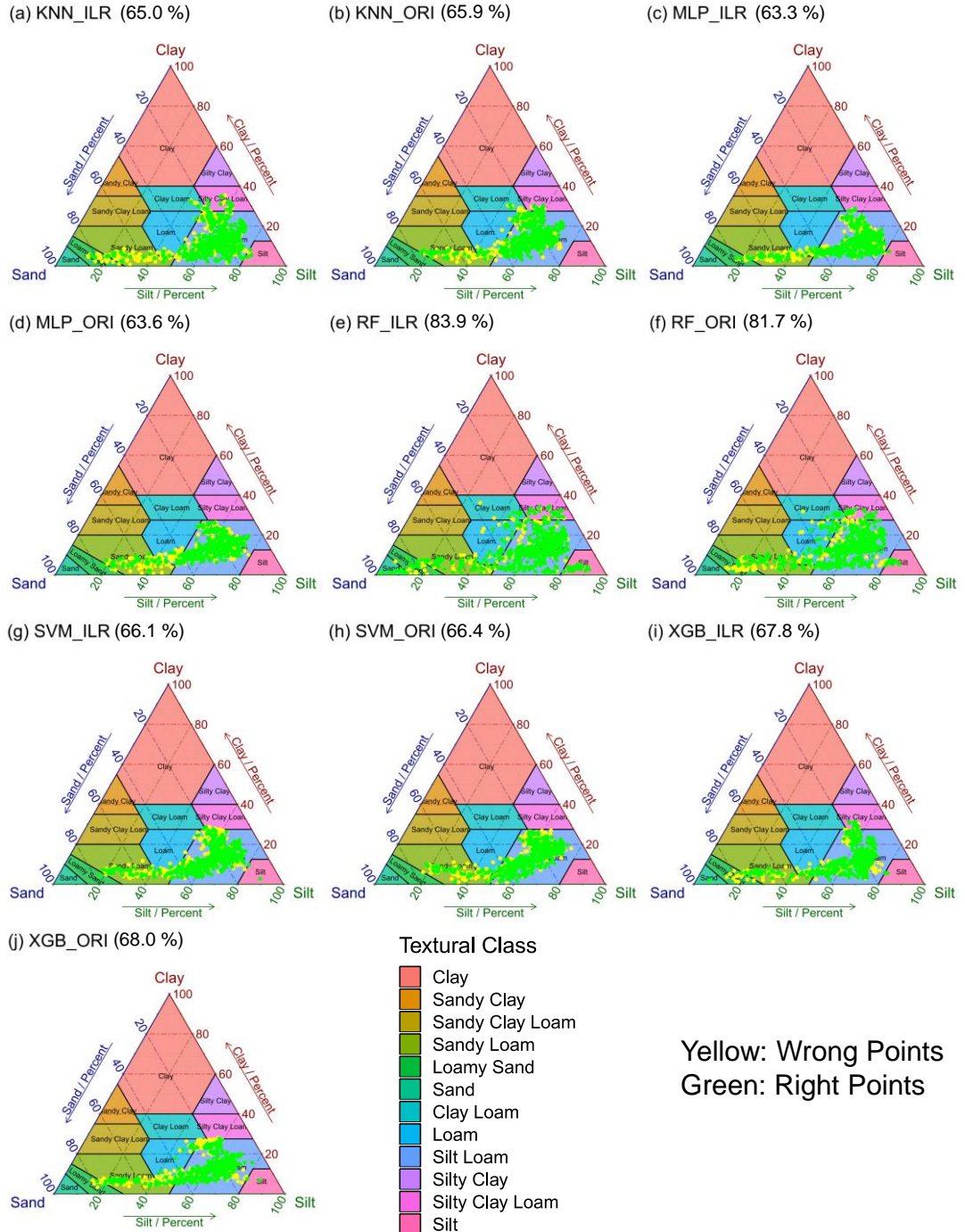


Figure 9. Soil texture types of 640 soil samples shown in USDA texture triangle. The results of soil PSF were generated from (a) KNN_ILR, (b) KNN_ORI, (c) MLP_ILR, (d) MLP_ORI, (e) RF_ILR, (f) RF_ORI, (g) SVM_ILR, (h) SVM_ORI, (i) XGB_ILR, and (j) XGB_ORI. Note that right points (green) mean that the predicted soil texture classes and these classes corresponding

to the original data were the same; wrong points (yellow) were the opposite, and the predicted right-ratios (RRs) of the soil texture types were in the bracket after interpolators in plots.”

Comment 3: The authors need to make it clear in the abstract (and discussion) what is their final conclusion considering: is transforming fractions necessary or not? which transformation is 'the best' (mapping accuracy wise)? what would you recommend as the best strategy to map PSFs / texture classes? and what are the most important implications of this work?

Response: Thanks for the referee's suggestions. We have deleted the sentence “Our systematic comparison helps to elucidate the processing and selection of compositional data in spatial simulation” and added the main conclusions, recommendation and implication of our work.

P20L28: *“With respect to the evaluation of accuracy, RF was recommended as the best strategy among these five machine-learning models according to soil PSF interpolation and soil texture classification. In addition, from the point of view of total computing time of model and sub-optimal accuracy (trade-offs of accuracy and time), XGB was preferred than any other models. Log ratio transformation methods were needed in the evaluation of the indirect soil texture classification and maps of PSFs and texture classes. Our findings can provide a reference for other research of spatial prediction of soil PSF and texture combined with environmental covariates using machine-learning methods with skewed distribution soil PSF data in a large area.”*

Comment 4: An additional recommendation, which is optional, is not to use Lat and Lon as predictors in a ML framework (it leads to obvious artifacts). Instead I would advise the authors to combine geographical distances to points, which is explained in detail in <https://peerj.com/articles/5518/> and which also helps solve problems of spatial autocorrelation etc. Again, this is optional recommendation and the paper would be equally useful without this adaptation. I also recommend looking at the work by Tolosana-Delgado et al. on interpolating compositional data (<https://link.springer.com/article/10.1007%2Fs11004-018-9769-3>), which is an important reference maybe missed by the authors.

Response: Thanks for the referee's constructive suggestion for removing Lat and Lon as covariates and the study of the interpolation of compositional data in soil science. Lat and Lon were used in our study, and artifacts were not obvious, which may because these two variables were not importance. If we delete Lat and Lon in our work, all consequences would be updated, and the workload is huge. However, it is a good advice and can guide our current research of regression kriging. Moreover, we have cited the reference “Geostatistics for Compositional Data: An Overview” and “Random forest as a generic framework for predictive modeling of spatial and spatio-temporal variables” in our revised version.

P22L22: *“Numerous different interpretations of the interpolation of compositional data in soil science have been suggested (Gobin et al., 2001; Lark and Bishop, 2007; Salazar et al., 2015; Tolosana-Delgado et al., 2019; Hengl et al., 2018)”*

Comments in the text

5 **Comment 1: P1L16: In this total, a total... typo.**

Response: Thanks for the referee's suggestion. We deleted "in this total" in our revised version.

P20L16: "*A total of 45 evaluation models generated from five different machine-learning models combined with original and three log ratio approaches—additive log ratio, centered log ratio and isometric log ratio (ALR, CLR and ILR, respectively)*"

10 **Comment 2: P1L19: modified the soil sampling...unclear sentence, you mean may be "decreased skewness of distributions"?**

Response: Thanks for the referee's question. Sentence "*the results demonstrated that log ratio approaches modified the soil sampling data more symmetrically*" means "*the results demonstrated that log ratio approaches decreased skewness of distributions of modified the soil sampling data*", we have modified this in our revised version.

15 **P20L19:** "*The results demonstrated that log ratio approaches decreased skewness of distributions of soil sampling data*"

Comment 3. P1L19: soil psf interpolation. please add here 1-2 sentences explaining the study area and data set used (number of points, area etc)

Response: Thanks for the referee's suggestion. We have improved this in our revised version.

20 **P20L18:** "*to evaluate and compare the performance of soil texture classification and soil PSF interpolation using 640 soil sampling data in the Heihe River Basin in China with an area of 146,700 km².*"

Comment 4: P1L20: showed notable consequences. vague; please rephrase using concrete stat measures.

Response: Thanks for the referee's suggestion. We have improved this in our revised version using concrete stat measures.

25 **P20L20:** "*with respect to soil texture classification, random forest (RF) and extreme gradient boosting (XGB) showed better consequences with the overall accuracy (RF: 0.629, XGB: 0.611), kappa coefficients (RF: 0.238, XGB: 0.240) and precision-recall curve (PRC) analysis (RF: 0.646, XGB: 0.616).*"

30 **Comment 5: P1L26: Our systematic comparison... Instead of this sentence (too subjective and not necessary) I would add the main conclusions (is transforming fractions necessary or not? What would you recommend as the best strategy to map PSFs / texture classes?) and implications of this work (to other peoples work).**

Response: Thanks for the referee's suggestion. We have deleted the sentence "Our systematic comparison helps to elucidate the processing and selection of compositional data in spatial simulation" and added the main conclusions, recommendation and implication of our work.

P20L28: "With respect to the evaluation of accuracy, RF was recommended as the best strategy among these five machine-learning models according to soil PSF interpolation and soil texture classification. In addition, from the point of view of total computing time of model and sub-optimal accuracy (trade-offs of accuracy and time), XGB was preferred than any other models. Log ratio transformation methods were needed in the evaluation of the indirect soil texture classification and maps of PSFs and texture classes. Our findings can provide a reference on spatial prediction of soil PSF and texture combined with environmental covariates using machine-learning methods with skewed distribution soil PSF data in a large area."

10

Comment 6: P2L1: (psf), better use capital letters "PSF" consistently

Response: Thanks for the referee's suggestion. We have improved this in our revised version.

Comment 7: P3L15: science have been suggested You missed an important reference:

<https://link.springer.com/article/10.1007%2Fs11004-018-9769-3>

Response: Thanks for the referee's suggestion for the study of the interpolation of compositional data in soil science, we have cited the reference "Geostatistics for Compositional Data: An Overview" and "Random forest as a generic framework for predictive modeling of spatial and spatio-temporal variables" in our revised version.

P22L22: "Numerous different interpretations of the interpolation of compositional data in soil science have been suggested (Gobin et al., 2001; Lark and Bishop, 2007; Salazar et al., 2015; Tolosana-Delgado et al., 2019; Hengl et al., 2018)"

Comment 8 and 9: P3L17: However, most studies using... Two times however, see next comment. P3L26: However, few studies combined... This repeats sentence in L17 on this page. I would recommend reducing the size of these paragraphs.

Response: Thanks for the referee's suggestion. We have reduced the size of the paragraph in our revised version, most of the deleted sentences were the description and comparison of kriging methods.

P22L27: "Huang et al. (2014) combined multiple linear regression with ALR to improve the prediction precision of soil PSF using electromagnetic data on a 1-m transect. Zhang et al. (2013) suggested compositional kriging was more appropriate for soil texture prediction than symmetry log ratio ordinary (or regression) kriging. Wang and Shi (2018) developed log ratio kriging combined with robust variogram estimation, which was preferable to compositional kriging methods. However, few studies combined log ratio with machine-learning models for soil PSF interpolation in soil science."

Comment 10: P4L13: direct soil texture classific... please explain for all readers what is "direct soil texture classification".

Response: Thanks for the referee's suggestion. The direct soil texture classification means predicting (or simulating) soil texture using texture classes as dependent variable, compared with the indirect soil texture classification (predicting soil texture by soil PSF interpolation).

P23L21: “to compare different performance of five machine-learning models in direct soil texture classification (soil texture classes as a dependent variable)”

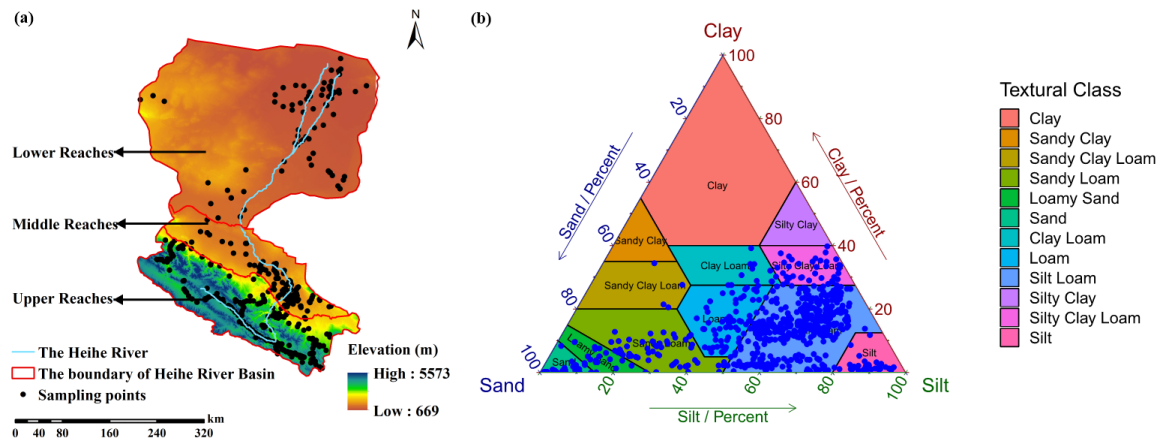
Comment 11: P4L24: -5-4 °C make difference between the minus sign and endash sign e.g. "-5 endash 4"

Response: Thanks for the referee's suggestion. We have improved this in our revised version, e.g. “-5—4 °C”

10 Comment 12: P5Fig1: These dots are beyond the cartographic scale of this visualization and should be removed. It politicizes the topic of soil texture mapping which is unnecessary. The topic of the paper is not the disputed islands but comparison of methods for PSF mapping.

Response: Thanks for the referee's suggestion. We have improved this figure in our revised version. We removed the geographical location of the Heihe River Basin in the origin fig. 1 (a) and added original soil PSF data (640 soil samples) in the USDA triangle.

P24L9:



“Figure 1. The (a) Heihe River, elevation and soil sampling points of Heihe River Basin, China and (b) these soil samples in the USDA triangle.”

Comment 13: P6L8, position information. this section needs to be extended - how was the sampling plan generated? did you sample per soil horizon or at fixed depths? did you take bulk samples or are the samples close-topoint support? Very important that all these things are clarified.

Response: Thanks for the referee's constructive comments, suggestions and questions, which can provide us encouragement to revise the paper to the best of our ability. We have added more details about soil samples such as the sampling strategy, sampling depth, sampling measurement, laboratory analysis methods and the average measurement error per texture fraction in our revised version.

5 **P25L22:** “*All soil samples had information about soil PSF (i.e., sand, silt and clay) using Malvern Mastersizer 2000 laser diffraction particle size analyzer (average measurement error is less than 3 %). The related environmental covariates were extracted using the extraction tool in ArcGIS, and the global position system (GPS) recorded the position information. Purposive sampling was used as the sampling strategy to collect soil samples and to characterize the spatial variability of soil PSF especially on such a regional scale of the study area (Zhu et al., 2008). In this strategy, sample sites were chosen based*

10 *on the variability of soil formation factors, which represented the heterogeneity of the soil PSF in the HRB such as the distribution of climate and categorical maps we mentioned, etc. To reduce the noise effect of soil sample, the average of mixed 3—5 topsoil (0—20 cm) samples for each soil sample and its parallel sample was used as the final measurement. Subsequently, the samples were dried, analyzed and measurement of soil PSF (approximately 30 g of each sample).*”

15 **Comment 14: P6L17: Latitude and longitude... I highly do not recommend using Lat and Lon as covariates. This has shown to lead to artifacts. For more details see: <https://peerj.com/articles/5518/>**

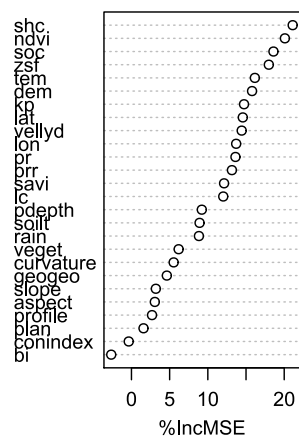
Response: Thanks for the referee's constructive suggestion for removing Lat and Lon as covariates. Lat and Lon were used in our study, and artifacts were not obvious, which may because these two variables were not importance. If we delete Lat and Lon in our work, all consequences would be updated, and the workload is huge. However, it is a good advice and can guide 20 our current research of regression kriging. We have cited it in our revised version.

Comment 15. P6L22: geomorphology types, soil... Please provide more detail - classes etc. Which soil map you used as covariate layer and how? Has this come up as a significant predictor?

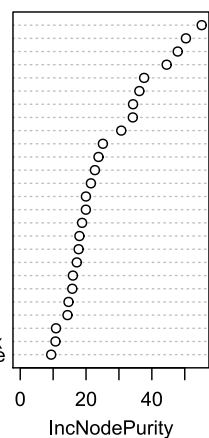
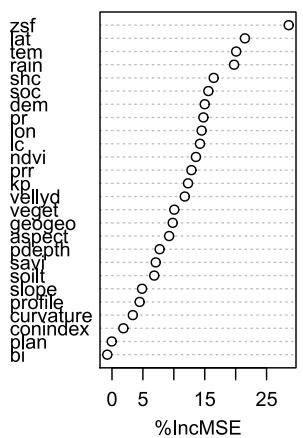
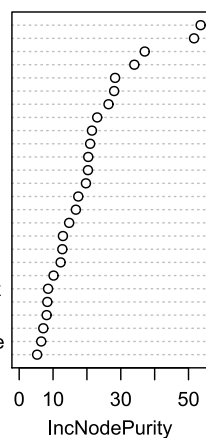
25 **Response:** Thanks for the referee's question. The maps of geomorphology types, soil types, land use types and vegetation types (Fig. 2) were added, revealing more detailed information of distribution of classes. The soil map was also demonstrated in Fig.2, which was described in our manuscript and used as categorical variable. Because these categorical maps were applied in previous research, showing close correlation with soil properties, these maps therefore were applied as environmental covariates. Moreover, before we produced our results, we did not know it was a significant predictor or not; the importance of environmental covariates can be generated from random forest model, which is shown as follows. These four categorical 30 variables (geo, lc, veget and soilt in figures) demonstrated moderate importance. However, it was not included in our work.

The importance of environmental covariates generated from RF (ILR / ORI):

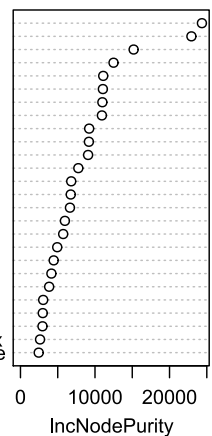
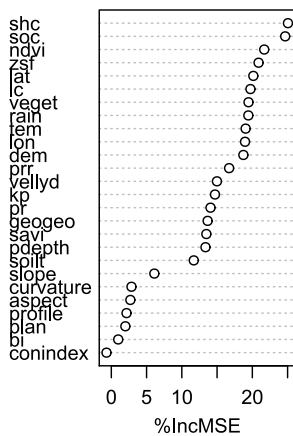
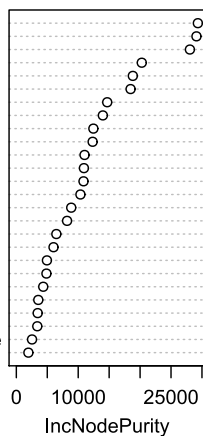
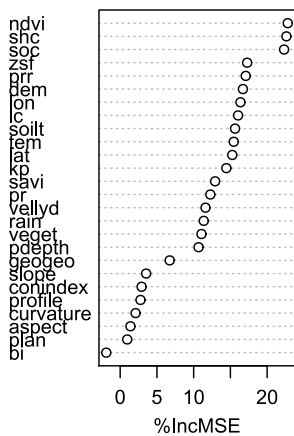
ILR_1RF



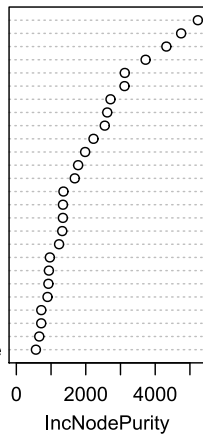
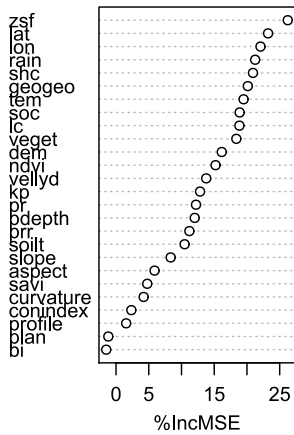
ILR_2RF



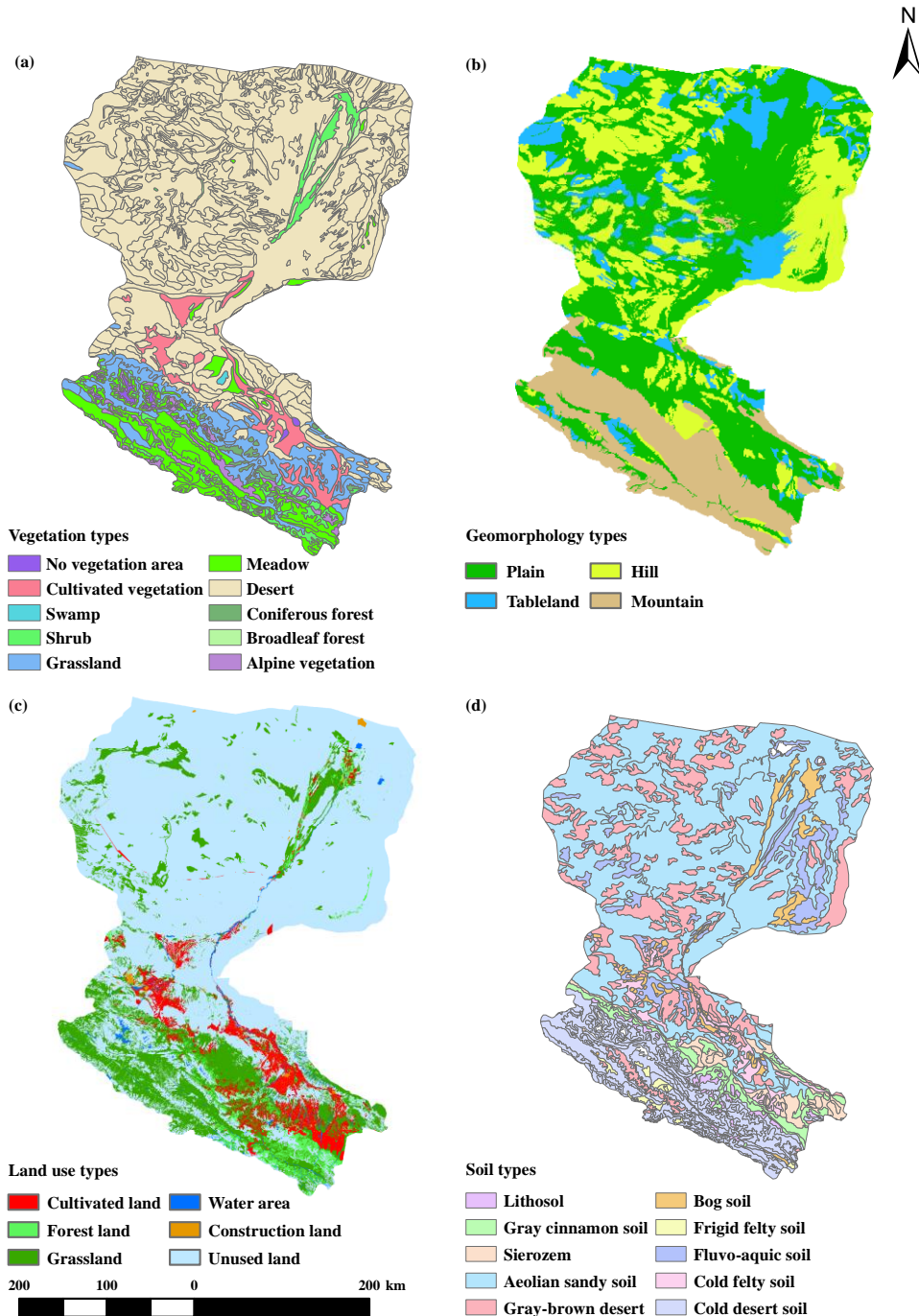
O_1RF



O_3RF



P27L1:



“Figure. 2. The spatial distributions of (a) vegetation types, (b) geomorphology types, (c) land use types and (d) soil types on the Heihe River basin.”

Comment 16: P7L6: the most popular multilayer... does Subasi (2007) claims that it is the most popular? Putting a reference here would be recommended.

Response: Thanks for the referee's question and suggestion for the reference, we have cited the reference of description of MLP model.

P28L11: "Multilayer perceptron neural network (MLP), which is currently one of the most popular multilayer feed forward backpropagation networks (Zhang et al., 2018; Gaurang et al., 2011), was selected to train artificial neural network (ANN) models in our study due to its rapid operation, small set of training requirements and ease of implementation (Subasi, 2007)."

Comment 17: P7L22: "randomForest" Unfortunately not optimized for larger data sets. I recommend using the "ranger" package instead.

Response: Thanks for the referee's suggestion. Considering the similarity of these two packages and the heavy workload of updated group figures, we did not replace "randomForest" with "ranger". However, the R package "ranger" can guide our future research of spatial prediction of soil PSF using RF model, especially with larger data sets.

Comment 18: P8L25: the other package of "randomForest", which package?

Response: Thanks for the referee's question. We apologized that it was our mistake, making the meaning confused. Here, we used the package "randomForest" for parameters optimization of RF, not the package "caret".

P30L1: "Thus, we used the package "randomForest" for RF and "kknn" for KNN, which can also restructure the parameters for these two models."

Comment 19: P10L16: 2008). I think the readers would appreciate here is you would explain how are the ALR/ILR numbers back-transformed to original 0-100% scale?

Response: Thanks for the referee's suggestion. We added the back-transformed equations for ALR, CLR and ILR transformation methods.

P31L21: "which were defined as follows:"

$$\overline{alr}(x_j) = \frac{\exp(alr(x_j))}{\sum_{j=1}^D \exp(alr(x_j))} , \quad (14)$$

$$\overline{clr}(x_j) = \frac{\exp(clr(x_j))}{\sum_{j=1}^D \exp(clr(x_j))} , \quad (15)$$

$$Y(x_j) = \sum_{j=1}^D \frac{ilr(x_j)}{\sqrt{j \times (j+1)}} - \sqrt{\frac{j-1}{j}} \times ilr(x_j) , \quad (16)$$

$$ilr(x_0) = ilr(x_D) = 0 , \quad (17)$$

$$\overline{ilr}(x_j) = \frac{\exp(Y(x_j))}{\sum_{j=1}^D \exp(Y(x_j))} , \quad (18)$$

Comment 20: P11L2: soil texture classification which soil.texture system have you used - USDA? Are you aware of the "soil.texture" package?

Response: Thanks for the referee's question. Yes, the soil texture system we used in our study was the USDA, and the R package "soiltexture" was mentioned in 2.6.4 (Indirect soil texture classification by soil PSF interpolation).

P35L19: "*thereafter; we transformed the content of three components (sand, silt and clay) into the soil texture types in the USDA soil texture classification using the R package "soiltexture" (Moeys, 2018).*"

Comment 21: P11L20: 0.01- 0.20: slight, ... Kappa depends on number of samples and number of classes - please clarify.

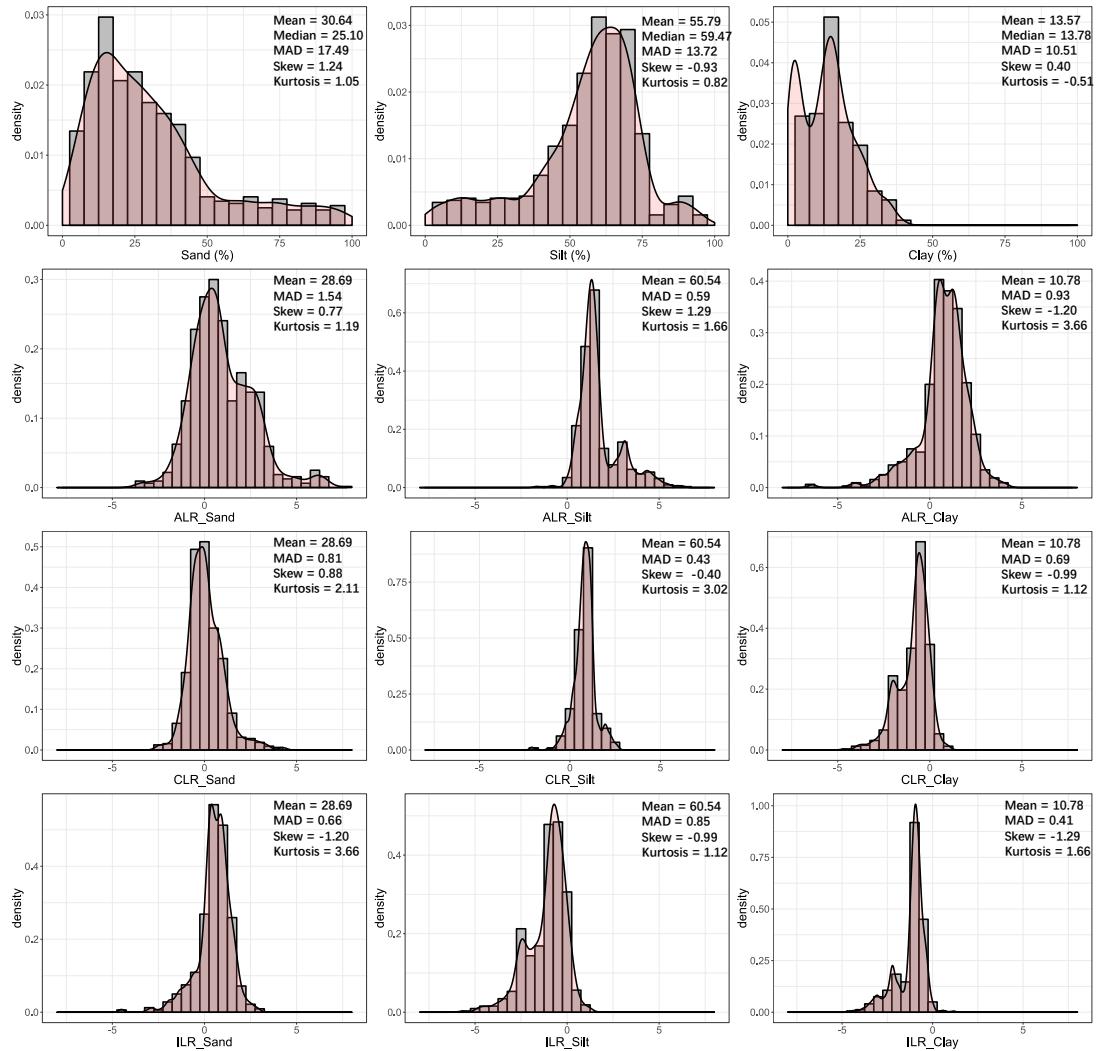
Response: Thanks for the referee's suggestion. Kappa depends on the confusion matrix, in the sentence "*When the numbers of samples in different classes are imbalanced in the data set, the kappa coefficient can explain the agreement of classes*", we wanted to emphasize that values of kappa coefficients can reveal more information (including the overall accuracy and more than that) based on imbalanced soil texture data than the overall accuracy, but it may not need to be stressed. The overall accuracy is important; however, when the number of samples are different for texture classes (imbalanced), for example, a certain class A dominates (more than half), and number of class B, C, D, E are less. Even though the prediction classes are all class A, the overall accuracy is more than 50 %, kappa is 0. We have modified this in our revised version.

P33L13: "*Kappa coefficient demonstrates the agreement of observed classes and measured classes*"

Comment 22: P15Fig2: This figure could be much improved: (1) put exactly the same scale (0-100% and -8 to 8 for the x-axis) so the distributions can be compared, (2) center all ALR, CLR and ILR plots at 0, (3) remove "Min" and "Max" from the labels (visible from the plots).

Response: Thanks for the referee's suggestion. We have improved this figure: put exactly the same scale (0-100% of sand, silt and clay and -8 to 8 for the x-axis), centered all ALR, CLR and ILR plots at 0, removed "Min" and "Max" from the labels.

P38L1:



“Figure 3. Descriptive statistical analysis for the original (untransformed) and log ratio transformed soil sampling data. Note that the means generated from log ratio transformed data were back-transformed to the real space.”

5 **Comment 23 and 24: P16L7: XGB plot shows "SVM" is the best? please check. P16FIG: Hmmm - SVM is both best and worst performing method based on this plot -please check.**

Response: Thanks for the referee's suggestion. We checked the results and these were right. For the overall accuracy, the values among five ML models were close, SVM showed the best performance; for the kappa, more fluctuation were revealed. In this boxplot, the most confusing results were two values of SVM—it was both best and worst performing method. In fact, 10 SVM only predicted two classes (nine classes in soil samples in total) of soil texture classes—SiLo and SaLo, both classes were dominant in our soil samples, the accuracy therefore was relatively high. However, kappa of SVM revealed more details

in imbalanced soil sampling data, which was the worst because SVM only predicted two main classes. Similar example was shown in the response of comment 21. We have mentioned this in our manuscript. From this point of view, we recommended using both the overall accuracy and kappa coefficients to evaluate soil texture classification.

P42L2: “*However, SVM predicted only two types, which was an unsatisfactory result associated with the lowest kappa coefficient*”

Comment 25.

P19FIG6: (image annotation) LoSa and SaLo are obviously most confused classes. But they are fairly similar to each other so not a big problem probably. To make that clear to readers I would use as legend the soil texture triangle as in <https://envirometrix.github.io/PredictiveSoilMapping/soilvariableschapter.html#convertingtexture-by-hand-classes-tofractions> (so that it is also visible which are the most similar classes).

Response: Thanks for the referee’s suggestion. We visited the website you gave and There were very detailed steps to convert texture classes to fractions. It can make readers to know the distribution of soil texture classes in the USDA triangles, like the small difference between LoSa and SaLo. However, in the direct soil texture classification, texture classes cannot be converted to soil PSF because of no information of soil PSF input (texture classes only). If only visualization of soil texture triangles and legend are needed, there were some soil texture triangles in our manuscript (Fig. 1 and Fig. 9) in the USDA system using the R package “ggplot2” and “ggttern”. We have added the description of the similarity of LoSa and SaLo in discussion part to make readers have more profound impression.

P56L1: “*In fact, LoSa and SaLo were obviously most confused classes; however, they are fairly similar to each other (see Fig. 1 or Fig. 9).*”

Comment 26: P21TABLE: The comparisons of accuracies... I would prefer again boxplots as in Fig. 3. Or at least put in bold the best performing methods please

Response: Thanks for the referee’s suggestion. We have improved this table, put in bold the best performing methods in our revised version.

Comment 27: P22L7: RF and XGB delivered more... Not substantiated. You mean more contrast / wider output distributions? Please rephrase.

Response: Thanks for the referee’s question. RF and XGB delivered prediction maps that were closer to the range of the distribution of original data, we have modified this in our revised version.

P45L6: “*RF and XGB delivered prediction maps that were closer to the range of the distribution of original data than did KNN, SVM and MLP.*”

Comment 28: P24L1: The interpolation maps... which methods have systematically underestimated / over-estimated sand content? which are most accurate? please add to the caption.

Response: Thanks for the referee's suggestion. We improved this part in our revised version. All the ranges of prediction maps of sand (approximately 9.0—90.0 %) were within the range of the original data (0.98—99.66 %), like the distribution of USDA triangles. Therefore, all models overestimated the low values and underestimated the high values. For sand content, maps of RF_ILR (7.9—94.7 %) and XGB_ORI (1.8—92.4 %) generated wider output distributions and were relatively closer to the range of the distribution of original data than other prediction maps such as KNN_ILR (7.3—88.6 %), KNN_ORI (7.8—80.8 %), MLP_ILR (8.8—90.8 %), MLP_ORI (9.0—90.3 %), RF_ORI (9.0—81.0 %), SVM_ILR (6.5—85.6 %), SVM_ORI (7.3—90.0 %) and XGB_ILR (5.0—88.5 %). From this point of view, RF and XGB were more accurate than others.

P47L1: *"All the ranges of prediction maps of sand (approximately 9.0—90.0 %) were within the range of the original data (0.98—99.66 %). RF_ILR (7.9—94.7 %) and XGB_ORI (1.8—92.4 %) generated wider output distributions and were relatively closer to the range of the distribution of original data than other prediction maps such as KNN_ILR (7.3—88.6 %), KNN_ORI (7.8—80.8 %), MLP_ILR (8.8—90.8 %), MLP_ORI (9.0—90.3 %), RF_ORI (9.0—81.0 %), SVM_ILR (6.5—85.6 %), SVM_ORI (7.3—90.0 %) and XGB_ILR (5.0—88.5 %)."*

Comment 29. P24TABLE: Overall accuracies and... Overall very small differences in performance. Why is that?

Response: Thanks for the referee's question, it can be explained from two aspect. First, the results of the indirect texture classification were generated from soil PSF interpolation, the values of soil PSF prediction among five ML models using different transformed data and original data were close (see indicators table), therefore different methods produced the same texture class, not crossing the texture boundary in the USDA system. Second, because of imbalanced soil texture (see response of comment 21) and "contraction effect" of prediction in the USDA triangles (see triangle figure) compared with the original data, there were very small differences of overall in performance.

Comment 30. P26 Figure 8. Soil This is an important figure. But it could be much improved: (1) text is too small (unreadable), (2) it is not clear what are the green and red colored points, (3) to each plot add some summary measure of performance (so we know which was best / worst). I would also move the (a) original data and put it into Fig. 1.

Response: Thanks for the referee's suggestion. We have improved this figure in our revised version. We made the text size larger, explained the meaning of yellow points and green points, added right ratios to compare different performance and removed the original data (a) and put it into Fig. 1.

P50L1:

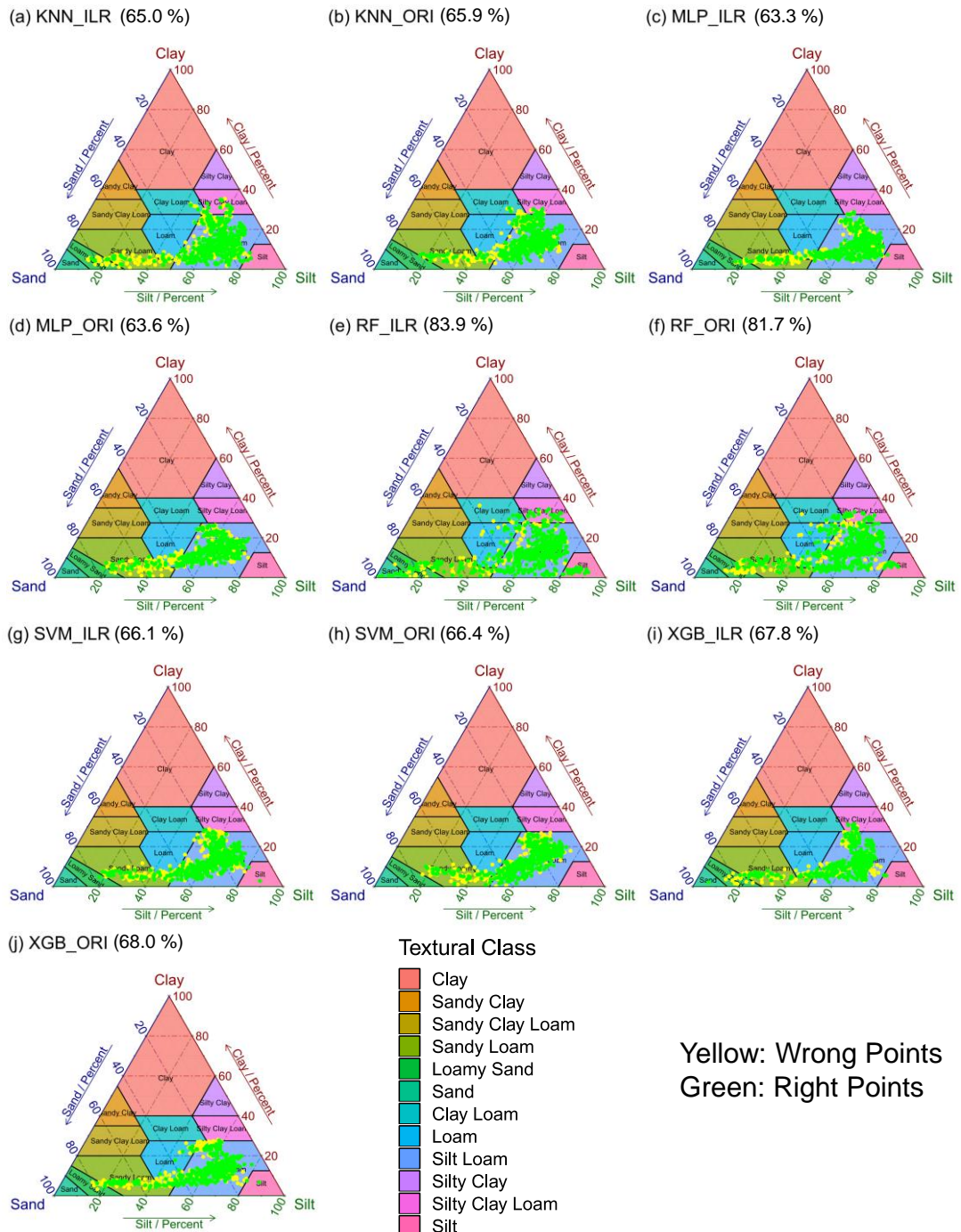


Figure 9. Soil texture types of 640 soil samples shown in USDA texture triangle. The results of soil PSF were generated from (a) KNN_ILR, (b) KNN_ORI, (c) MLP_ILR, (d) MLP_ORI, (e) RF_ILR, (f) RF_ORI, (g) SVM_ILR, (h) SVM_ORI, (i) XGB_ILR, and (j) XGB_ORI. Note that right points (green) mean that the predicted soil texture classes and these classes corresponding

to the original data were the same; wrong points (yellow) were the opposite, and the predicted right-ratios (RRs) of the soil texture types were in the bracket after interpolators in plots.”

Comment 31. P28FIG9: see my comment on Fig. 6.

5 **Response:** Thanks for the referee’s suggestion. Please see the response of comment 25.

Comment 32: P29L3: time-spending, total computing time.

Response: Thanks for the referee’s suggestion. We improved this part in our revised version.

P53L3: “*Comparison of total computing time for each model in soil texture classification and soil PSF interpolation*”

10

Comment 33. P29FIG10: mention how many trees you use? If you reduce the standard number of trees to e.g. 80 you do not loose much on accuracy but the computing time drops significantly.

15

Response: Thanks for the referee’s question, for RF model, 1000 trees were used because of the parameter’s adjustment (2.4.6 Parameters optimization). Therefore, only optimization parameters were taken into account for each model. However, it is constructive advice and we added it in discussion part.

P54L25: “*For the total computing time, RF revealed the longest time with respect to both classification (453.73 s) and regression (188.87 s); moreover, 1000 trees were used because of the parameter’s adjustment. However, the computing time may drop significantly and accuracy do not lose much by reducing the number of trees, which need to be considered in future research.*”

20

Comment 34. P31L7: however, this improvement... please elaborate - what do you mean by "not greatly effective"?

25

30

Response: Thanks for the referee’s question. The interpretation of “not greatly effective” means although log ratio transformed data was superior to the original data according to descriptive statistics, log ratio cannot make 640 soil sampling data become normal distribution and these transformed data cannot pass the k-s test because of outliers. To show the true environmental distribution, we did not remove these outliers. Further, from the view of the parameter adjustment, because of the small range of log ratio transformed data, when these parameters were fixed within certain ranges, the values of assessment indicators (e.g. MEs, RMSEs, etc.) remain stable (small values) and the same rule were obtained. However, when the prediction values of log ratio methods were back-transformed to the real space, these indicators (e.g. MEs, RMSEs, etc.) will be enlarged. Moreover, there has been concern that the optimal estimate of log ratio transformed data does not deliver the optimal estimate of the compositions back-transformed to the real space. In the process of parameters optimization, the optimal parameters of different machine-learning methods using log ratio transformed data were obtained; however, it cannot guarantee that the values of assessment indicators were optimal using these parameters when independent data set were used to validate the models. Thus, the “optimal” does not seem very significant for parameter adjustment of log ratio data.

P55L9: “however, this improvement was not greatly effective because of outliers, in order to show the true environmental distribution, we did not remove these outliers. Fig.2 illustrated that soil sampling data for sand and clay were right-skewed, and silt was left-skewed because the silt component was predominant. The ALR transformed method enhanced soil sampling data of sand; nevertheless, the ALR_sand was still right-skewed, similar to the CLR_sand, presenting the lack of adjustment.

5 In contrast, the ILR_sand changed from right-skewed to left-skewed; from this point of view, the over-adjustment was revealed. Similarly, the lack of adjustments was also shown in CLR_silt and ILR_silt; over-adjustments included ALR_silt, ALR_clay, CLR_clay and ILR_clay, making images that were different from normal distribution, and the p values of k-s tests were not significant.”

10

Comment 35: P32L26: more symmetric distribution... I am not sure what you mean here - PSF's are given and cannot be manipulated?

Response: Thanks for the referee’s question. Here we mean more efficient soil PSF data transformation methods and we have modified this part in our revised version.

15 **P56L30:** “More appropriate environmental covariates and interpolation techniques, more efficient soil PSF data transformation methods (or multiple perspectives of compositional data selection), and systematic parameter adjustment algorithms of compositional data are key to improving accuracy in the future.”

20 **Comment 36. P32L30: Data availability. The... I checked the links and they are (1) made for Chinese users only, (2) require registration / username+pw. I would recommend putting instead the whole project and data on Github + zenodo.org.**

Response: Thanks for the referee’s suggestion. Publishing soil sampling data from the website requires data usage protocol. We cannot public the data because we do not have the right, because we are just users of data and should obey the protocol.

Systematic comparison of five machine-learning methods in classification and interpolation of soil particle size fractions using different transformed data

Mo Zhang^{1,2}, Wenjiao Shi^{1,3}

5 ¹Key Laboratory of Land Surface Pattern and Simulation, Institute of Geographic Sciences and Natural Resources Research, Chinese Academy of Sciences, Beijing 100101, China

²School of Earth Sciences and Resources, China University of Geosciences, Beijing 100083, China

³College of Resources and Environment, University of Chinese Academy of Sciences, Beijing 100049, China

Correspondence to: Wenjiao Shi (shiwj@lreis.ac.cn)

10 **Abstract.** Soil texture and soil particle size fractions (psfPSF) play an increasing role in physical, chemical and hydrological processes. Digital soil mapping using machine-learning methods was widely applied to generate more detailed prediction of qualitative or quantitative outputs than traditional soil-mapping methods in soil science. As compositional data, interpolation of soil psfPSF combined with log ratio approaches was developed to improve the prediction accuracy, which also can be used to indirectly derive soil texture. However, few reports systematically analyzed and compared the classification and regression, 15 the accuracies of original (untransformed) and log ratio approaches, and the performance of direct and indirect soil texture classification using machine-learning methods. ~~In this total, a~~A total of 45 evaluation models generated from five different machine-learning models combined with original and three log ratio approaches—additive log ratio, centered log ratio and isometric log ratio (ALR, CLR and ILR, respectively), to evaluate and compare the performance of soil texture classification and soil psfPSF interpolation using 640 soil sampling data in the Heihe River Basin in China with an area of 146,700 km². The 20 results demonstrated that log ratio approaches decreased skewness of distributions of modified the soil sampling data ~~more symmetrically~~, and with respect to soil texture classification, random forest (RF) and extreme gradient boosting (XGB) showed notable consequences with the overall accuracy (RF: 0.629, XGB: 0.611), kappa coefficients (RF: 0.238, XGB: 0.240) and precision-recall curve (PRC) analysis (RF: 0.646, XGB: 0.616). For soil psfPSF interpolation, RF delivered the best 25 performance among five machine-learning models with lowest root mean squared error (RMSE, sand: 15.09 %, silt: 13.86 %, clay: 6.31 %), mean absolute error (MAE, sand: 10.65 %, silt: 9.99 %, clay: 5.00 %), Aitchison distance (AD, 0.84) and standardized residual sum of squares (STRESS, 0.61), and highest coefficient of determination (R^2 , sand: 53.28 %, silt: 45.77 %, clay: 53.75 %). STRESS was improved using log ratio approaches, especially CLR and ILR. There is a pronounced improvement (21.3 %) in the kappa coefficient using indirect soil texture classification compared to the direct approach. With respect to the evaluation of accuracy, RF was recommended as the best strategy among these five machine-learning models according to soil PSF interpolation and soil texture classification. In addition, from the point of view of total computing time of model and sub-optimal accuracy (trade-offs of accuracy and time), XGB was preferred than any other models. Log ratio transformation methods were needed in the evaluation of the indirect soil texture classification and maps of PSFs and texture

classes. Our findings can provide a reference for other research of spatial prediction of soil PSF and texture combined with environmental covariates using machine-learning methods with skewed distribution soil PSF data in a large area. Our systematic comparison helps to elucidate the processing and selection of compositional data in spatial simulation.

1 Introduction

5 Soil texture, classified by ranges of soil particle-size fractions (psfPSF), is one of the most important attributes affecting the soil properties and the physical, chemical and hydrological processes covering soil porosity, soil fertility, water retention, infiltration, drainage and aeration. Measuring soil texture can be used for soil fertility management (Pahlavan-Rad and Akbarimoghaddam, 2018), water management (Thompson et al., 2012), maintenance of organic carbon (Bationo et al., 2007) and provision of ecosystem services (Adhikari and Hartemink, 2016). The soil psfPSF, i.e., sand, silt and clay, are vital in most 10 hydrological, ecological, and environmental risk assessment models (Liess et al., 2012). The spatial distributions of soil texture and soil psfPSF affect and control runoff generation, slope stability, depth of accumulation, and soluble salt content (McNamara et al., 2005; Follain et al., 2006; Yoo et al., 2006; Gochis et al., 2010; Crouvi et al., 2013).

15 Previous reports revealed that there are close correlations between the spatial variations of soil texture and landscape and topography (Gobin et al., 2001; Brown et al., 2004; Zhao et al., 2009; Liess et al., 2012). Compared with traditional soil mapping methods, digital soil mapping (DSM) has an obvious advantage in that it is considerably more economical and efficient; additionally, soil maps using DSM yielded more details because of the development of data-mining algorithms and 20 GIS tools and more extensive application of spatial remote sensing data, particularly in the regional and continental scale. DSM methods were applied by an increasing number of soil scientists to map soil properties using ancillary data (McBratney et al., 2003; Zeraatpisheh et al., 2017), the so-called environmental covariates, which can be obtained from digital elevation models (DEM), remote sensing data, and categorical or geomorphology maps (Krasilnikov et al., 2011). Furthermore, some

1 Abbreviations: psfPSF, soil particle-size fractions; HRB, Heihe River Basin; DSM, digital soil mapping; KNN, k-nearest neighbor; MLP, multilayer perceptron neural network; RF, random forest; SVM, support vector machines; XGB, extreme gradient boosting; ALR, additive log-ratio; CLR, centered log-ratio; ILR, isometric log-ratio; ORI, original; ROC, receiver operating characteristics; PRC, precision-recall curve; AUC, area under the ROC curve; AUPRC, area under the PRC; RMSE, root mean squared error; MAE, mean absolute error; R², coefficient of determination; MAD, median absolute deviation; AD, Aitchison distance; STRESS, standardized residual sum of squares; KNN_ALR, KNN_CLR, KNN_ILR, KNN_ORI, MLP_ALR, MLP_CLR, MLP_ILR, MLP_ORI, RF_ALR, RF_CLR, RF_ILR, RF_ORI, SVM_ALR, SVM_CLR, SVM_ILR, SVM_ORI, XGB_ALR, XGB_CLR, XGB_ILR, XGB_ORI, KNN, MLP, RF, SVM, XGB combined with ALR, CLR, ILR, ORI respectively; ClLo, clay loam; Lo, loam; LoSa, loamy sand; Sa, sand; SaClLo, sandy clay loam; SaLo, sandy loam; Si, silt; SiClLo, silty clay loam; SiLo, silt loam.

soil physicochemical attributes, such as soil organic carbon (SOC) and pH, were also permissible to obtain as environmental covariates (Camera et al., 2017). Wang and Shi (2017) also recommended that the soil ~~psfPSF~~ prediction should consider the ancillary data, which can enhance the performance of interpolation.

Different machine-learning methods, such as boosting regression trees (Jafari et al., 2014; Yang et al., 2016), random forests (Hengl et al., 2015; Zeraatpisheh et al., 2017) and artificial neural networks (Bagheri Bodaghabadi et al., 2015; Taalab et al., 2015), have been most commonly employed in DSM models for both regression and classification combined with environmental covariates in soil science. Hengl et al. (2015) contrasted the performance of spatial predictions of soil properties, such as soil ~~psfPSF~~, using random forests and linear regression, and the results demonstrated that the random forests were superior to the linear regression with remarkable advantages of not only robust to noise but also low bias and variance. Hengl et al. (2017) improved the prediction of organic carbon, bulk density, pH and soil texture fractions on a global scale using machine-learning models – random forest, gradient boosting and multinomial logistic regression – indicating that random forest and gradient boosting outperformed linear models in large data sets. Taghizadeh-Mehrjardi et al. (2015) investigated the predictive power of soil classes using six machine learning-based classifiers and found that artificial neural network and decision trees performed better than any other models they mentioned with relatively high overall accuracies and kappa coefficients. Heung et al. (2016) evaluated a suite of 10 machine-learning models for predicting soil taxonomic units, and the consequences suggested that although the k-nearest neighbor and support vector machine had the highest accuracy, “tree learners” were preferred because of the interpretability of the results and the speed of parameterization. Most previous studies selected one or more machine-learning algorithms to simulate soil category or continuous variables for classification or regression problems. From this perspective, however, few studies systematically analyzed both soil texture classification and soil ~~psfPSF~~ interpolation using multiple machine-learning methods.

The soil ~~psfPSF~~, which can be classified as soil texture, are not only continuous variables but also compositional data. We need to pay more attention to the latter case. Numerous different interpretations of the interpolation of compositional data in soil science have been suggested (Gobin et al., 2001; Lark and Bishop, 2007; Salazar et al., 2015; [Tolosana-Delgado et al., 2019](#); [Hengl et al., 2018](#)), and the most extensively used were a combination of log ratio approaches involving the additive log ratio (ALR) and the centered log ratio (CLR) put forward by Aitchison (1982), as well as the isometric log ratio (ILR) from Egozcue et al. (2003). ~~However, most studies using log ratio approaches to simulate the spatial variation of soil psf were kriging methods (so-called geostatistics), rather than machine learning methods.~~ Huang et al. (2014) combined multiple linear regression with ALR to improve the prediction precision of soil ~~psfPSF~~ using electromagnetic data on a 1-m transect. ~~Odeh et al. (2003) proposed that modified ALR ordinary kriging transcended compositional kriging and cokriging. Sun et al. (2014) contradistinguished compositional kriging, log ratio cokriging, cokriging, and ALR cokriging, and produced proximate results. In contrast, Walvoort and de Gruijter (2001) thought compositional kriging had better performance than ALR ordinary kriging.~~ Zhang et al. (2013) suggested compositional kriging was more appropriate for soil texture prediction than symmetry log ratio ordinary (or regression) kriging. Wang and Shi (2018) developed log ratio kriging combined with robust variogram estimation,

which was preferable to compositional kriging methods. However, few studies combined log ratio with machine-learning models for soil ~~psfPSF~~ interpolation in soil science. Aside from those mentioned above, the lack of systematic comparison of accuracy, strengths and weaknesses between original (untransformed) and log ratio approaches should be considered, especially in terms of combining with machine-learning methods.

Soil texture classification using machine-learning methods can be classified as a dependent variable; furthermore, it also can be derived indirectly from soil ~~psfPSF~~. Camera et al. (2017) reported that random forests were more remarkable than multinomial logistic regression in the direct soil texture classification. Wu et al. (2018) compared the support vector machines (SVM), artificial neural network (ANN), and classification tree (CT) models, demonstrating better prediction performance generated from SVM than from CT and ANN. For the indirect classification of soil texture, Poggio and Gimona (2017) combined hybrid geostatistical generalized additive models with ALR and modeled soil particle classes at medium resolution (250 m) in Scotland, expecting that vegetation index, morphological features and information about the phenological season were of vital significance as environmental covariates. Considering the particularity of compositional data, the consequences of soil ~~psfPSF~~ classification and regression (indirect soil texture classification and soil ~~psfPSF~~ interpolation, respectively) could be compared from the direct and indirect soil texture classification as a result of the relationship between soil texture and soil ~~psfPSF~~. Nevertheless, few studies systematically compared these using different machine-learning methods combined with original (untransformed) and log ratio transformed data for both direct and indirect soil texture classification.

In our study, five machine-learning models – k-nearest neighbor (KNN), multilayer perceptron neural network (MLP), random forest (RF), support vector machines (SVM), and extreme gradient boosting (XGB) – were included and applied for DSM of soil texture classification and soil ~~psfPSF~~ interpolation. Furthermore, the original (untransformed) and log ratio transformed data were also combined with the machine-learning algorithms mentioned above for soil ~~psfPSF~~ interpolation. Hence, the objectives of this study are (i) to compare different performance of five machine-learning models in direct soil texture classification ([soil texture classes as a dependent variable](#)), (ii) to evaluate the accuracies of different log ratio approaches and original (untransformed) method applied for soil ~~psfPSF~~ from the perspective of compositional data using machine-learning models, and (iii) to estimate whether the accuracies of indirect soil texture classification using original (untransformed) data and log ratio transformed data were improved compared with the direct soil texture classification.

2 Data and methods

2.1 Study area

The Heihe River Basin (HRB, 97°6'—102°3' E, 37°43'—42°40' N) is situated in the Hexi Corridor, northwest of China, covering the Inner Mongolia Autonomous Region, Gansu and Qinghai provinces ([Fig. 1a](#)), which is the second largest inland river basin in China with an area of 146,700 km². The elevation and three reaches (i.e., upper, middle and lower) of the study area are shown in Fig. [1b1a](#). For the upper reaches of HRB, the climate changes significantly with altitude; the mean annual

precipitation is 350 mm, the mean annual temperature is from -5—4 °C and the annual average evaporation is 1000 mm. For the middle reaches of HRB, the mean annual precipitation declines between 250 and 50 mm, the annual average evaporation increases from 2000 (east) to 4000 mm (west), and the mean annual temperature is from 2.8 to 7.6 °C. The lower reaches of HRB are situated in Ejina Banner on the Alxa Plateau, which is an arid desert climate with annual precipitation under 50 mm and annual average evaporation above 3500 mm; the mean annual temperature is from 8 to 10 °C.

5

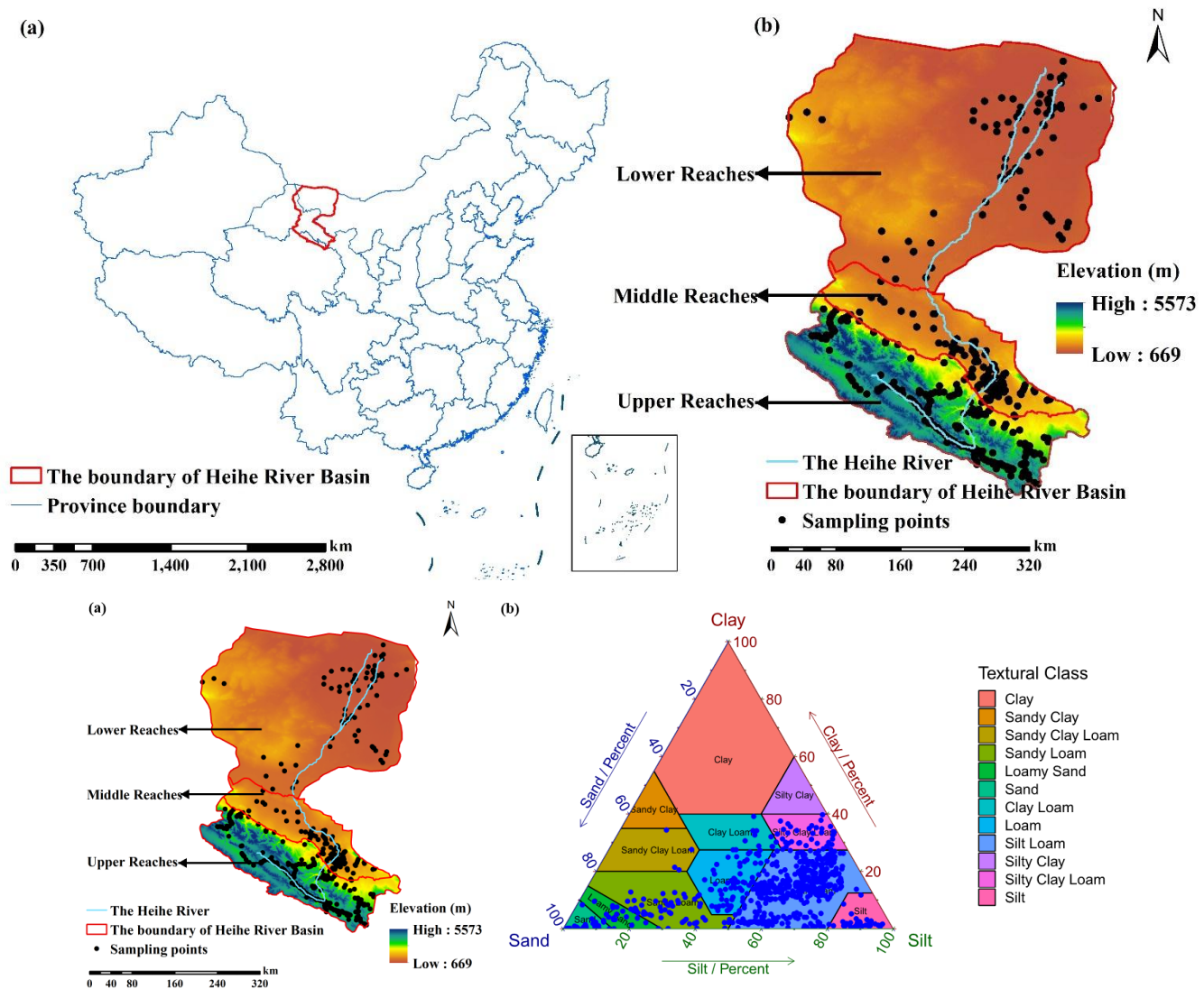


Figure 1. The (a) geographical location, (b) Heihe River, elevation and soil sampling points of Heihe River Basin, China.

Figure 1. The (a) Heihe River, elevation and soil sampling points of Heihe River Basin, China and (b) these soil samples in the USDA triangle.

10

The vegetation of the upper reaches of HRB is influenced from the southeast to northwest by hydrothermal conditions. The main vegetation types are alpine vegetation (4000—5000 m), alpine meadow vegetation belt (3000—4000 m), alpine shrub meadow (3200—3800 m), mountain forest meadow belt (2400—3200 m), mountain grassland belt (1800—2400 m), and desert base belt (less than 1800 m). The main vegetation types of the middle and lower reaches of the HRB are relatively fewer, including cultivated vegetation and desert, and the areas near the Heihe River on the lower reaches are shrub and steppe.

The main soil types are frigid desert soils (less than 4000 m), alpine meadow soil and alpine steppe soil (3600—4000 m), gray cinnamon soil and chernozem (3200—3600 m), sierozem and ~~gray cinnamon soil~~~~chestnut soil~~ (2600—3200 m), ~~gray cinnamon soil~~~~chestnut soil~~ (2300—2600 m) and sierozem (1900—2300 m) on the upper reaches of the HRB. The main soil types on the middle reaches of HRB are aeolian sandy soil, frigid frozen soil and gray brown desert soil. The main soil types in the lower reaches of HRB are aeolian sandy soil, gray brown desert soil (northwest) and lithosol (northeast).

The main types of geomorphology on the upper reaches of HRB are modern glaciers, alpine and hilly, and plimatic basins. Narrow plains are distributed on the middle reaches of HRB. For the lower reaches, the main types of geomorphology are hilly (northwest), plain, sandy land and platform (east), and the area near Heihe River is a flood plain.

2.2 Soil sampling

A total of 640 soil sampling points was collected in the HRB from the Science Data Center of Cold and Arid Regions (WestDC) in China (<http://westdc.westgis.ac.cn/>), involving 392 soil sampling points on the upper reaches and 248 soil sampling points on the middle and lower reaches of the HRB. The soil types, vegetation types, distribution of DEM and geomorphology types of the HRB were considered in soil sample collection according to the location and proportion of these types for the purpose of more representative spatial characteristics of soil ~~psf~~~~PSF~~ using limited soil samples. There were more soil sampling points on the middle and upper reaches of HRB due to the more complicated soil types and vegetation types in these areas. In contrast, the types on the lower reaches are relatively similar with more desert in the northwest. Hence, the east of the lower reaches of the HRB contained more soil sampling points. All soil samples had information about soil PSF (i.e., sand, silt and clay) using Malvern Mastersizer 2000 laser diffraction particle size analyzer (average measurement error is less than 3 %). The related environmental covariates were extracted using the extraction tool in ArcGIS, and the global position system (GPS) recorded the position information. Purposive sampling was used as the sampling strategy to collect soil samples and to characterize the spatial variability of soil PSF especially on such a regional scale of the study area (Zhu et al., 2008). In this strategy, sample sites were chosen based on the variability of soil formation factors, which represented the heterogeneity of the soil PSF in the HRB such as the distribution of climate and categorical maps we mentioned, etc. To reduce the noise effect of soil sample, the average of mixed 3—5 topsoil (0—20 cm) samples for each soil sample and its parallel sample was used as the final measurement. Subsequently, the samples were dried, analyzed and measurement of soil PSF (approximately 30 g of each sample). All soil samples had information about soil psf~~PSF~~ (i.e., sand, silt and clay) and related environmental covariates

~~using a laser diffraction approach and the extraction tool in ArcGIS, respectively, and the global position system (GPS) recorded the position information.~~

2.3 Environmental covariates and pre-processing

The environmental covariates, such as topographic attributes, remote sensing attributes, climate and position attributes, soil physicochemical attributes and categorical maps, are logically related to the distributions of soil ~~psfPSF~~. System for Automated Geoscientific Analysis (SAGA) GIS (Conrad et al., 2015) was used to compute their topographic attributes from DEM, including slope, aspect, convergence index, curvature, plane curvature, profile curvature and valley depth. Remote sensing attributes, including the normalized difference vegetation index (NDVI, Huete et al., 2002), the Brightness index (BI, Metternicht and Zinck, 2003), and the soil adjusted vegetation index (SAVI, Huete, 1988) were derived from the Landsat 7 based on band operation. We also collected climate attributes from the National Meteorological Information Center (NMIC, <http://data.cma.cn/>), such as the mean annual precipitation and the mean annual temperature. Latitude and longitude were also considered because of the large scale of the HRB. Mean annual surface evapotranspiration data (Wu et al., 2012) were gathered from WestDC (<http://westdc.westgis.ac.cn/>), as were soil physicochemical attributes, such as soil organic carbon, saturated water content, field water holding capacity, wilt water content, saturated hydraulic conductivity, and soil thickness (Yi et al., 2015; Song et al., 2016; Yang et al., 2016), which can address the distributions of soil ~~psfPSF~~, as well. Additionally, the categorical maps, which were of significance, such as geomorphology types, soil types, landcoveruse types and vegetation types (Fig. 2, were also used). For slope, the method of dividing the hierarchy rotates clockwise from the north (0°), and each 45° was an interval, including north (337.5—22.5°), northeast (22.5—67.5°), east (67.5—112.5°), southeast (112.5—167.5°), south (167.5—202.5°), southwest (202.5—247.5°), west (247.5—292.5°), and northwest (292.5—337.5°).

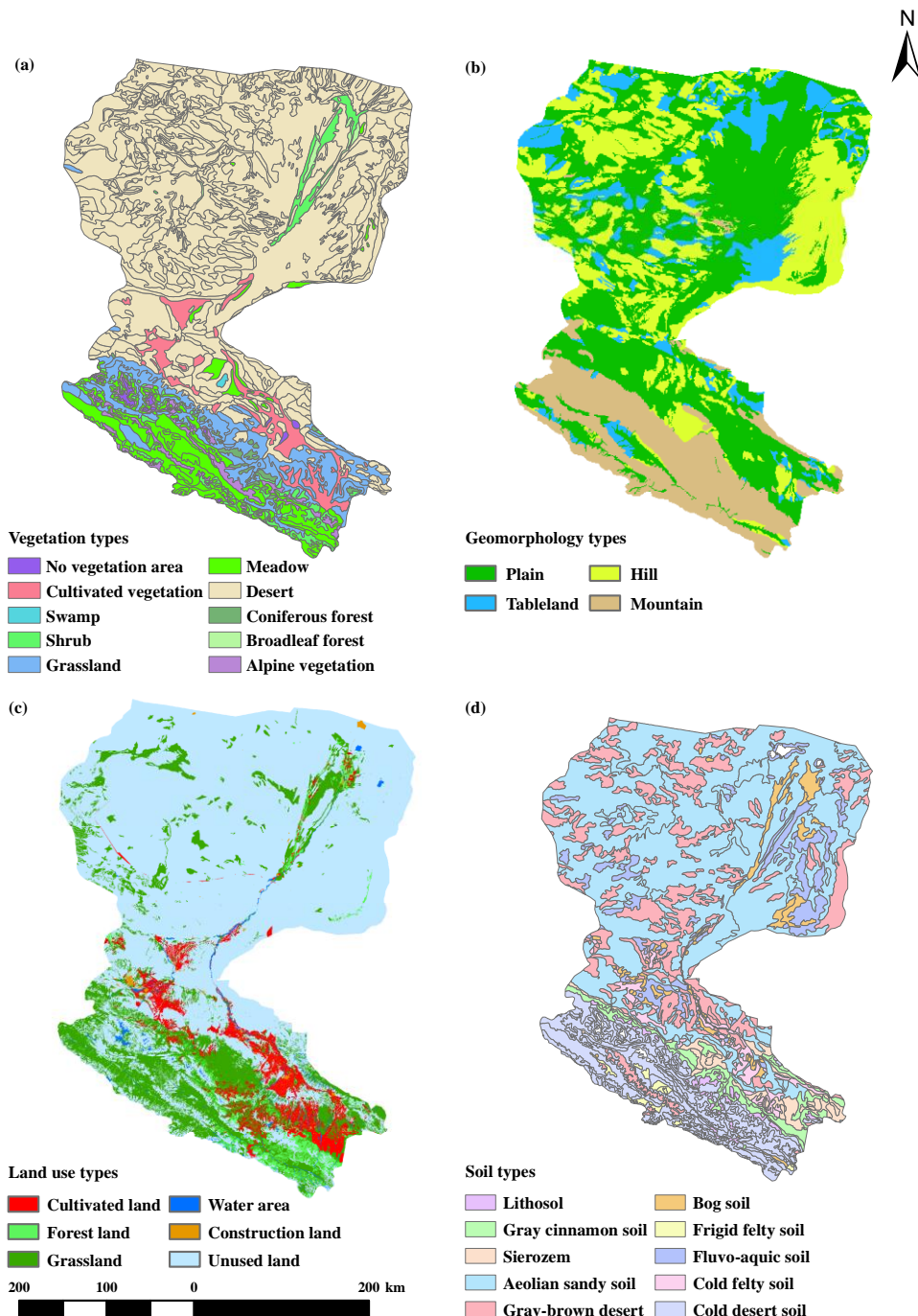


Figure 2. The spatial distributions of (a) vegetation types, (b) geomorphology types, (c) land use types and (d) soil types on the Heihe River basin.

2.4 Machine learning methods and parameters optimization

2.4.1 K-nearest neighbor (KNN)

K-nearest neighbor (KNN) is a simple non-parametric classifier based on known instance to label unknown instance (Cover and Hart, 1967). For the test set, k-nearest training set vectors were found, and maximum summed kernel densities were computed for classification. Moreover, continuous variables can also be predicted for regression with the average values of k-nearest neighbors. Weighted KNN is an extended version of KNN that considers the distances of the nearest neighbors; therefore, the parameters of KNN contain the maximum value of k (kmax), the distances of the nearest neighbors (distance) and the types of kernel function (kernel). The KNN model is available in the R package “kknn” (Schliep and Hechenbichler, 2016).

10 2.4.2 Multilayer perceptron neural network (MLP)

Multilayer perceptron neural network (MLP), which is currently one of the most popular multilayer feed forward backpropagation networks ([Zhang et al., 2018](#); [Gaurang et al., 2011](#)), was selected to train artificial neural network (ANN) models in our study due to its rapid operation, small set of training requirements and ease of implementation (Subasi, 2007). MLP neurons can perform classification or regression depending on whether the response variable is categorical or continuous.

15 The MLP has three sequential layers: input layer, hidden layer and output layer. The resilient backpropagation algorithm was chosen because the learning rate of this algorithm is adaptive, avoiding oscillations and accelerating the learning process (Behrens and Scholten, 2006). The range of the data set should be standardized because MLPs operate in terms of the scale 0 to 1. MLP can be run using the R package “RSNNS” (Bergmeir and Benitez, 2012).

2.4.3 Random forest (RF)

20 Random forest (RF) was developed by Breiman (2001), combining the bagging method (Breiman, 1996) with the random variable selection, and the principle was to merge a group of “weak learners” together to form a “strong learner”. Bootstrap sampling is used for each tree of RF, and the rules to binary split data are different for regression and classification problems. For classification, the Gini index is used to split the data; for regression, minimizing the sum of the squares of the mean deviations can be selected to train each tree model. Benefits of using RFs are that the ensembles of trees are used without 25 pruning. In addition, RF is relatively robust to overfitting, and standardization or normalization are not necessary because it is insensitive to the range of value. Two parameters should be adjusted for RF model: the number of trees (ntree) and the number of features randomly sampled at each split (mtry). The RF model is available in the R package “randomForest” (Liaw and Wiener, 2002).

2.4.4 Support vector machines (SVM)

The support vector machine (SVM), proposed by Cortes and Vapnik (1995), is a type of generalized linear classifier that is widely applied for classification and regression problems in soil science (Burges, 1998). The main principle of SVM is to classify different classes by constructing an optimal separating hyperplane in the feature space (so called “structural risk minimization”). Regression problems also can be solved by minimization of the structural risk using loss functions (Vapnik, 1998) in SVM, named support vector regression. The advantages of SVMs are that they are effective in high dimensional spaces. Radial basis function was selected for SVM as the kernel function in our study, and two other parameters need to be tuned, i.e., cost and gamma, controlling the tradeoff between the classification accuracy and complexity, and the ranges of radial effect, respectively. The SVM model is available in the R package “e1071” (Meyer et al., 2017).

10 2.4.5 Extreme gradient boosting (XGB)

Extreme Gradient Boosting, put forward by Chen and Guestrin (2016), is an efficient method of implementation for gradient boosting frames, tree learning algorithms and efficient linear model solvers to solve both classification and regression problems (Chen et al., 2018). Like the boosted regression trees (Elith et al., 2008), it follows the principle of gradient enhancement; however, more regularized model formalization is applied to XGB to control over-fitting, making it more remarkable. In addition, parallel calculations can be automatically executed during the training phase of the XGB model, presenting a great advantage in large data sets, as the XGB can be more than ten times faster than the existing gradient boosting model (Chen and Guestrin, 2016). There are seven parameters should be tuned in XGB, containing the learning rate (eta), the maximum depth of a tree (max_depth), the max number of boosting iterations (nrounds), the subsample ratio of columns (colsample_bytree), the subsample ratio of the training instance (subsample), the minimum loss reduction (gamma) and the minimum sum of instance weight (min_child_weight). The XGB model is available in the R package “xgboost” (Chen et al., 2018).

2.4.6 Parameters optimization

The parameters of machine-learning models we mentioned above need to be adjusted, and the numbers of these parameters of models are different. For instance, XGB has seven parameters and is one of the most complicated models; on the other hand, for the MLP, in the case where we have chosen the algorithm, the only parameter that should be tuned is the size of the MLP model.

R package “caret” (Kuhn, 2018) provides an effective grid-search method that can automatically adjust the parameters by setting the adjustment grid, avoiding the uncertainty of artificial adjustment for some models (e.g., XGB) with more parameters. A set of parameters with the lowest RMSE or the highest R^2 for regression and the highest overall accuracy or kappa coefficient for classification by cross-validation can be selected to be the best parameters. However, in the presence of many adjustment

parameters, it may be inefficient due to the long training time. Thus, we used the ~~other~~ package ~~of~~ “randomForest” for RF and “kknn” for KNN, which can also restructure the parameters for these two models.

In our study, eleven dependent variables (i.e., ten for regression and one for classification) were trained with environmental covariates (independent variables) for the sake of parameter adjustment for each model, including “sand, silt, clay, ilr1, ilr2, alr1, alr2, clr1, clr2, clr3” and “class”. Subsequently, the parameters were definitely computed; here, we just give the relative ranges of the parameters after adjustment for most dependent variables; for example, in KNN the kmax was 15, the distance was 1, and the kernel was rectangular; in MLP, the size fluctuated between 5 and 10; in RF, the ntree was 1000 and mtry fluctuated from 9 to 11; in SVM, gamma was 0.01 and cost was 1; and in XGB, the range of parameters of max_depth (3 ~~—~~ 4), eta (0.05 ~~—~~ 0.1), colsample_bytree (0.6 ~~—~~ 0.8), nrounds (30), subsample (0.8 ~~—~~ 1), gamma (0 ~~—~~ 0.4), and min_child_weight (0.6 ~~—~~ 0.8) were obtained after conditioning.

2.5 Log-ratio transformation methods

For soil ~~psfPSF~~ compositional data (i.e. sand, silt and clay), the sum of the components is 1 (or 100 %), which should be guaranteed. Soil particle size data, including three dimensions, are typical compositional data. The closed number system can be explained as follows: the individual variables in the data set are not independent of each other; moreover, they are related by being expressed as a percentage (Filzmoser et al., 2009). In the Euclidean space, one dimension (variable) would be omitted for the original method to guarantee no information loss because of the constant-sum constraint. Therefore, the Euclidean space is not appropriate for the analysis of soil ~~psfPSF~~ data. The most widely used approaches are log ratio approaches (Aitchison, 1982), consisting of the additive log ratio, centered log ratio and isometric log ratio (ALR, CLR and ILR for short, respectively) from Aitchison (1982) and Egozcue et al. (2003).

For the composition of D elements $\mathbf{x} = [x_1, \dots, x_D]$, $x_j > 0$, $\forall j = 1, \dots, D$, and $\sum_{j=1}^D x_j = 1$, the transformation equation for ALR is defined as follows:

$$alr(\mathbf{x}) = (\ln \frac{x_1}{x_j}, \dots, \ln \frac{x_{j-1}}{x_j}, \ln \frac{x_{j+1}}{x_j}, \dots, \ln \frac{x_D}{x_j}), \quad (1)$$

For soil ~~psfPSF~~ ($D = 3$) in our study, the transformation equations for ALR are:

$$alr(1) = \ln \frac{\text{sand}}{\text{clay}}, \quad (2)$$

$$alr(2) = \ln \frac{\text{silt}}{\text{clay}}, \quad (3)$$

All of the information regarding the soil ~~psfPSF~~ was contained in $alr(1)$ and $alr(2)$; however, the ALR has been criticized because the choice of denominator is subjective, which can influence the results (Bacon-Shone, 2011). The CLR transformation method can remove this arbitrariness, and the equation is defined as follows

$$clr(\mathbf{x}) = (y_1, \dots, y_j, \dots, y_D) = (\ln \frac{x_1}{\sqrt[D]{\prod_{j=1}^D x_j}}, \dots, \ln \frac{x_D}{\sqrt[D]{\prod_{j=1}^D x_j}}), \quad (4)$$

where y_j is the j th component. Similarly, for the soil ~~psfPSF~~, the transformation equations for CLR are:

$$clr(1) = \ln \frac{\text{sand}}{\sqrt[3]{\text{sand} \times \text{silt} \times \text{clay}}}, \quad (5)$$

$$clr(2) = \ln \frac{\text{silt}}{\sqrt[3]{\text{sand} \times \text{silt} \times \text{clay}}}, \quad (6)$$

$$clr(3) = \ln \frac{\text{clay}}{\sqrt[3]{\text{sand} \times \text{silt} \times \text{clay}}}, \quad (7)$$

In the CLR transformation method, the geometric mean composed of all compositions of soil psfPSF is the denominator, and one-to-one mapping of equations and soil psfPSF could be implemented. Nevertheless, the CLR is inapplicable for multivariate analysis because the sum of the dimensions of CLR is 0, and thus the results are collinear. These problems can be overcome by using ILR, which transforms all the information into D-1 orthogonal log contrasts (Abdi et al., 2015). The transformation equations for ILR are defined as follows:

$$\mathbf{z} = (z_1, \dots, z_{D-1}) = ilr(\mathbf{x}), \quad (8)$$

$$z_i = \sqrt{\frac{D-i}{D-i+1}} \ln \frac{x_i}{\sqrt[D-i]{\prod_{j=i+1}^D x_j}}, \text{ for } i = 1, \dots, D-1, \quad (9)$$

where z_i is the i th component. The ILR transformation equations for soil psfPSF in our study can also be defined as follows:

$$ilr(1) = \sqrt{\frac{2}{3}} \ln \frac{\text{sand}}{\sqrt{\text{silt} \times \text{clay}}}, \quad (10)$$

$$ilr(2) = \sqrt{\frac{1}{2}} \ln \frac{\text{silt}}{\text{clay}}, \quad (11)$$

For a more uniform comparison of the descriptive statistics, the ordering of three components of soil psfPSF followed sand-silt-clay, and we added the third equation for the ALR and ILR. Although all the information could be included in the first two equations, note that in the process of interpolation, only the first two equations were used for ALR and ILR:

$$alr(3) = \ln \frac{\text{clay}}{\text{sand}}, \quad (12)$$

$$ilr(3) = \sqrt{\frac{2}{3}} \ln \frac{\text{clay}}{\sqrt{\text{sand} \times \text{silt}}}, \quad (13)$$

The equations for $alr(1), alr(2), alr(3)$ were equivalent to $alr(\text{sand}), alr(\text{silt}), alr(\text{clay})$ in ALR, the same as in ILR.

The back-transformed equations for ALR, CLR and ILR were recommended in our previous research (Wang and Shi, 2017), and were computed in the “compositions” R package (van den Boogaart and Tolosana-Delgado, 2008), which were defined as follows:

$$\overline{alr}(x_j) = \frac{\exp(alr(x_j))}{\sum_{j=1}^D \exp(alr(x_j))}, \quad (14)$$

$$\overline{clr}(x_j) = \frac{\exp(clr(x_j))}{\sum_{j=1}^D \exp(clr(x_j))}, \quad (15)$$

$$Y(x_j) = \sum_{j=1}^D \frac{ilr(x_j)}{\sqrt{j \times (j+1)}} - \sqrt{\frac{j-1}{j}} \times ilr(x_j), \quad (16)$$

$$ilr(x_0) = ilr(x_D) = 0, \quad (17)$$

$$\overline{ilr}(x_j) = \frac{\exp(Y(x_j))}{\sum_{j=1}^D \exp(Y(x_j))}. \quad (18)$$

For the original (untransformed) method, the standardization function was used to ensure predictions of soil **psfPSF** were between 0 and 100 and that their sum was 100%:

$$sand_s = \frac{sand}{(sand+silt+clay)} \times 100,$$

5 (4419)

where, $sand_s$ is the content of sand after standardization, the same as silt and clay component.

2.6 Validation

2.6.1 Validation method

A total of 45 methods that we simulated are presented in Table 1; five machine-learning models were combined with one original (ORI) and three log ratio approaches (ALR, CLR, ILR). Five machine-learning methods were applied for direct soil texture classification; additionally, these methods were combined with original (untransformed) and log ratio transformed data for a total of 40 methods for indirect soil texture classification (20) and soil **psfPSF** interpolation (20). The data were randomly divided into two sets to guarantee prediction accuracies; for instance, one (70 % = 448 soil samples) was employed for training models and the other (30 % = 192 soil samples) was set aside for validation. This process was repeated 30 times for soil texture classification and soil **psfPSF** interpolation, and different indicators were chosen to evaluate different performances of models (or methods).

Table 1. The method system of soil texture classification and soil **psfPSF** interpolation.

Methods	Soil texture classification		Soil psfPSF interpolation
	Direct classification	Indirect classification	
Original data (ORI)	KNN, MLP, RF, SVM, XGB	KNN_ORI, MLP_ORI, RF_ORI, SVM_ORI, XGB_ORI	—
Log-ratio transformed data (ALR, CLR, ILR)	—	KNN_ALR, KNN_CLR, KNN_ILR, MLP_ALR, MLP_CLR, MLP_ILR, RF_ALR, RF_CLR, RF_ILR, SVM_ALR, SVM_CLR, SVM_ILR, XGB_ALR, XGB_CLR, XGB_ILR,	

2.6.2 Validation indicators for soil texture classification

The overall accuracy (Brus et al., 2011) and kappa coefficient were selected to evaluate the overall effects of soil texture types predicted by different models. Moreover, the receiver operating characteristic (ROC) curve, precision-recall curve (PRC), area under the ROC curve (AUC), area under the precision-recall curve (AUPRC) and abundance index were applied to evaluate the performance of different soil texture types.

The overall accuracy represents all samples of soil texture types correctly classified by machine-learning models, divided by the total number of samples of soil texture types used in the validation. The higher overall accuracy, the more accurate soil map (Brus et al., 2011):

$$\text{Overall Accuracy} = \frac{TP+TN}{TP+TN+FP+FN},$$

(4520)

where T, F, P and N denote True, False, Positive, and Negative and TP, TN, FP, FN were true positive, true negative, false positive, and false negative. ~~When the numbers of samples in different classes are imbalanced in the data set, the kappa coefficient can explain the agreement of classes (Marchetti et al., 2011)~~ Kappa coefficient demonstrates the agreement of observed classes and measured classes, which is calculated based on the confusion matrix, the equation is defined as:

$$\kappa = \frac{p_o - p_e}{1 - p_e},$$

(4621)

where, p_o is the probability of observed agreement (overall accuracy) and p_e is the probability of agreement when two classes are unconditionally independent. The strength of the kappa coefficients is interpreted in the following manner: 0.01—-0.20: slight, 0.21—-0.40: fair, 0.41—-0.60: moderate, 0.61—-0.80: substantial, 0.81—-1.00: almost perfect (Landis and Koch, 1977).

The probabilities of different soil texture types (sum to 1) obtained during the training and predicting processes of machine-learning models were selected to calculate the sensitivity, specificity, precision and recall:

$$\text{Sensitivity} = \text{recall} = \frac{TP}{TP+FN},$$

(4722)

$$\text{Specificity} = \frac{TN}{TN+FP},$$

(4823)

$$\text{Precision} = \frac{TP}{TP+FP},$$

(4924)

In general, sensitivity, precision and recall indicate the extent of identifying positive cases, and specificity demonstrates the extent of identifying the negative cases of models. ROC analysis is commonly used in two-class problems. However, soil

texture types are more than two classes. In our point of view, a one-vs-rest strategy was employed to produce different ROC graphs for each soil texture type.

$$P_i = c_i,$$

(2025)

$$5 \quad N_i = \bigcup j \neq i c_j \in C,$$

(2426)

where C is the set including all classes, P_i is the positive class, N_i is the negative class, including all classes except c_i in ROC graph i (Fawcett, 2006).

In practice, the weakness of the ROC curve is that it cannot indicate the differences among the models in the cases of imbalanced samples between positive and negative. Soil texture data are a class-imbalanced data set of positive and negative, and the negative classifier would be overvalued under these circumstances because of the overabundance of majority (negative) examples, additionally revealing overly optimistic findings (Davis and Goadrich, 2006). However, precision and recall curves (PRC) are more informative than ROC curves in dealing with class-imbalanced data (Fu et al., 2017). The R package “precrec” (Saito and Rehmsmeier, 2017) generated ROC and PRC curves and computed AUC and AUPRC for each soil texture type.

This process was repeated 30 times and eventually, the average ROC and PRC curves with their average areas under these curves were obtained.

Abundance index was applied to describe the proportion of all soil texture types and well-classified soil texture types in the prediction map, which was defined as follows:

$$Abundance\ index = p/t,$$

(2227)

where p is all soil texture types in the prediction map and t is well-classified soil texture type(s) in test sets. For the sake of ensuring the balance of the soil texture types, all nine soil texture types were involved in test sets, covering clay loam (ClLo: 12), loam (Lo: 57), loamy sand (LoSa: 18), sand (Sa: 23), sandy clay loam (SaClLo: 4), sandy loam (SaLo: 58), silt (Si: 31), silty clay loam (SiClLo: 37), and silt loam (SiLo: 400); most were SiLo (62.5%) and the fewest were SaClLo (0.63%).

25 2.6.3 Validation indicators for soil ~~psf~~PSF interpolation

The accuracy and performance of machine-learning models mentioned above for the original (untransformed) and different log ratio transformation approaches were evaluated using five statistical indicators, containing coefficient of determination (R^2), root mean square error (RMSE), mean absolute error (MAE), Aitchison distance (AD, Aitchison, 1992), and standardized residual sum of squares (STRESS, Martin-Fernandez et al., 2001). The equations for the validation indicators R^2 , RMSE, MAE, AD and STRESS are as follows:

$$R^2 = \frac{\sum_{i=1}^n (Y_{i,m} - Y_{i,e})}{\sum_{i=1}^n (Y_{i,m} - \bar{Y}_{i,m})},$$

(2328)

$$RMSE = \sqrt{\frac{1}{n} \sum_{i=1}^n (Y_{i,m} - Y_{i,e})^2},$$

(2429)

$$MAE = \frac{1}{n} \sum_{i=1}^n |Y_{i,m} - Y_{i,e}|,$$

(2530)

where $Y_{i,m}$, $Y_{i,e}$, $\bar{Y}_{i,m}$ and n are the measured, predicted and the mean of measured soil **psfPSE** and the number of observations (soil sampling points for validation). Closer to 1 and higher values of R^2 and the lower values of RMSE and MAE show better performance of models and methods.

$$AD = \left[\sum_{i=1}^D \left[\log \frac{x_i}{g(x)} - \log \frac{x_i}{g(X)} \right]^2 \right]^{1/2},$$

(2631)

$$STRESS = \left[\frac{\sum_{i < j} (AD_{x,ij} - AD_{X,ij})^2}{\sum_{i < j} (AD_{x,ij})^2} \right]^{1/2},$$

(2732)

where x is the observed value; X is the predicted value; D is the number of dimensions (for soil **psfPSF** is 3); $g(x)$ denotes the geometric mean $(x_1 \dots x_D)^{1/D}$; $AD_{x,ij}$ and $AD_{X,ij}$ are the ADs between the observed soil **psfPSE** and the predicted soil **psfPSF** at sites i and j . Both present that model performances are better when the values are lower.

2.6.4 Indirect soil texture classification by soil **psfPSF** interpolation

Seventy percent of the 640 soil sampling points were used for training each machine-learning model, and the remaining 30 % were used for the soil **psfPSE** interpolation; thereafter, we transformed the content of three components (sand, silt and clay)

into the soil texture types in the USDA soil texture classification using the R package “soiltexture” (Moeys, 2018). Eventually, the overall accuracy and kappa coefficient were computed and evaluated. This process was repeated 30 times, and the averages of these consequences were employed to compare the classification performance of each model. The direct and indirect soil texture classifications were also compared with the overall accuracy and kappa coefficient. The training and testing sets for each time were the same by setting seeds, and all calculations and analysis were performed with the freely available software

R (R Core Team, 2018).

2.7 Statistical analysis for the original and log-ratio transformed data

The mean, median, minimum (Min), maximum (Max), median absolute deviation (MAD), skewness (Skew), kurtosis and Kolmogorov-Smirnov test ($p > 0.05$) were employed for descriptive statistical analysis of the original (untransformed) and log ratio transformed soil **psfPSF** data. The arithmetic mean of log-ratio transformation data should be back-transformed to the original space. For $X = [X_1, \dots, X_n]$, the MAD can be calculated according to the Eq. (28) as below:

$$MAD(X) = median(|X_i - median(X)|).$$

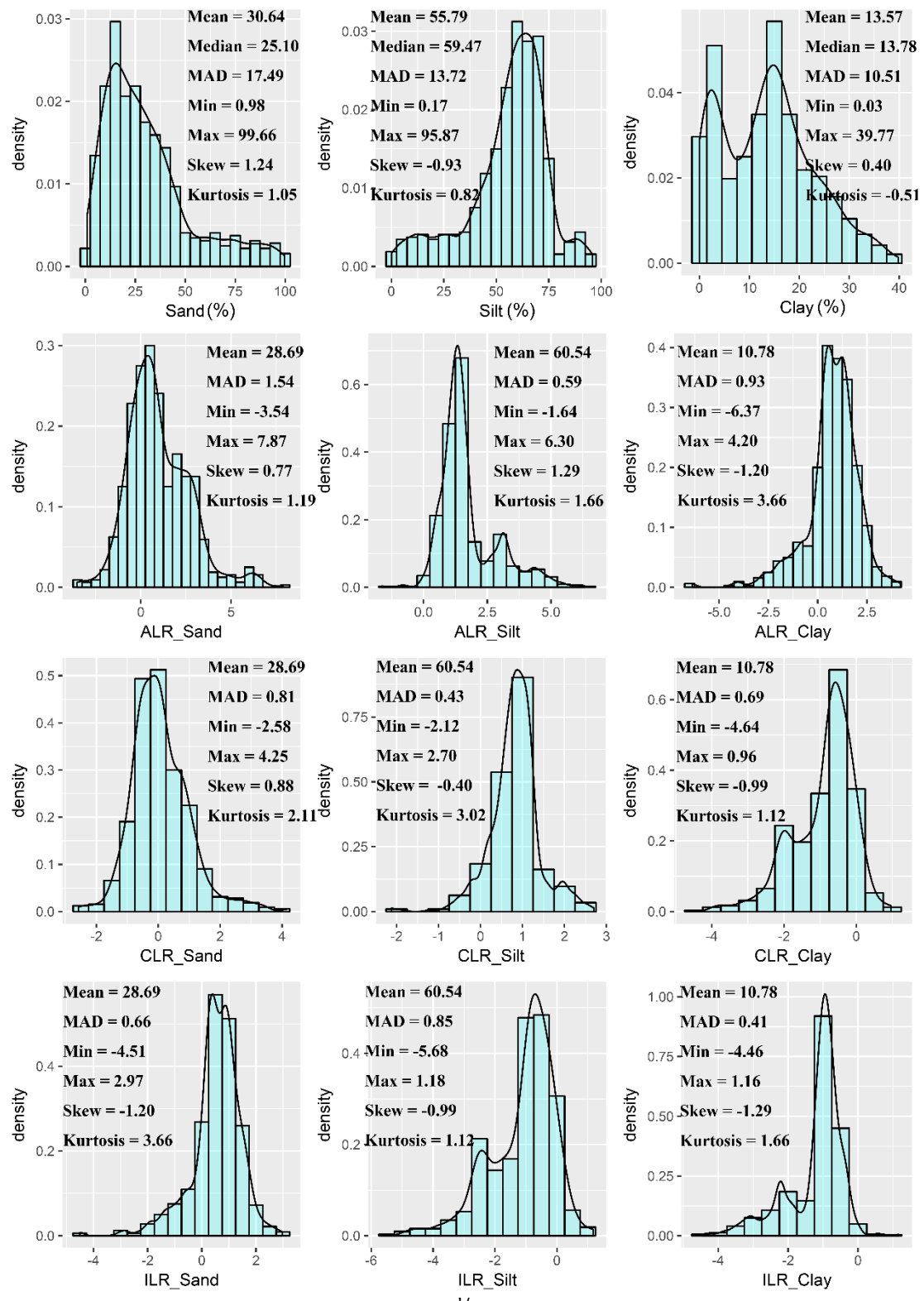
(2833)

3 Results

3.1 The descriptive statistics for the original and log-ratio transformed soil **psfPSF** data

With respect to the original (untransformed) data of sand, the mean fraction (30.64 %) was much higher than that of median fraction (25.10 %); conversely, both silt and clay were the opposite, with lower mean fractions (silt: 55.79 %, clay: 13.57 %) than median fractions (silt: 59.47 %, clay: 13.78 %). For the log ratio transformed data, the means of sand (28.69 %) and silt (60.54 %) were closer to the median values of the original data, aside from clay, with mean of 10.78 %.

All MADs of log ratio transformed data were much smaller than those of the original data in all cases; for instance, ILR contained the best value of MAD for sand (0.66) and clay (0.44), and CLR generated the lowest MAD for silt (0.43) among different log ratio approaches (Fig. 23). All log ratio approaches had lower skews (ALR: 0.77, CLR: 0.88, ILR: -1.20) than those of the original data (1.24) for sand. Moreover, CLR (-0.4) declined the original skew (-0.93) for silt. However, it was negligible for log ratio transformation data compared with the original skew of clay (0.4). The kurtosis of all log ratio approaches was much higher compared with the consequences generated from original (untransformed) data. In terms of the k-s test ($p < 0.05$), although the p values of the original (untransformed) and different log ratio transformed data were not significant and all histograms were not subject to normal distribution, log ratios made the images of the data more symmetric (Fig. 23).



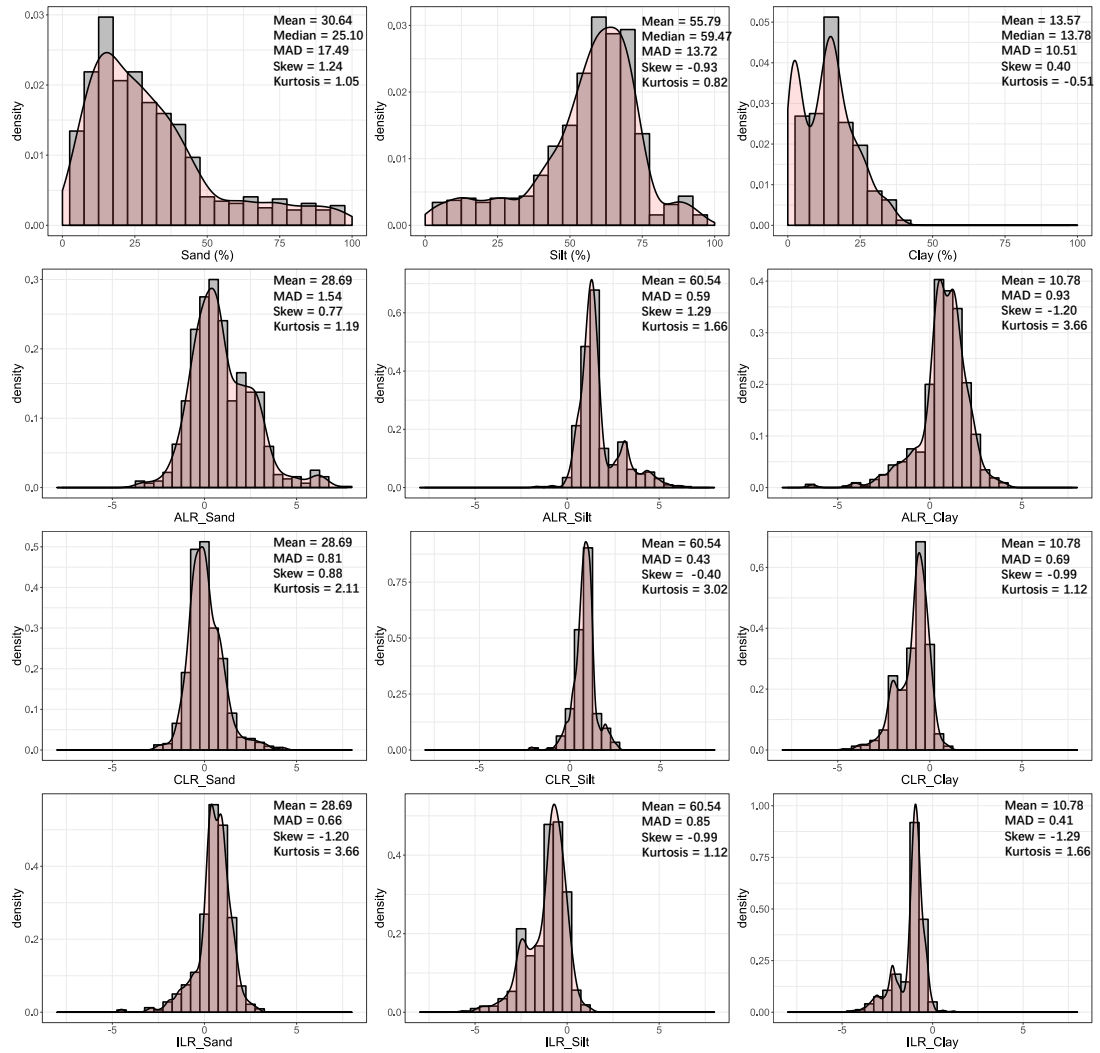


Figure 23. Descriptive statistical analysis for the original (untransformed) and log_{ratio} transformed soil sampling data. Note that the means generated from log ratio transformed data were back-transformed to the real space.

3.2 Comparison of the machine learning models in the classification of soil texture types

5 3.2.1 Comparison of the validation indicators for soil texture classification

The overall accuracy of each model ranged from 0.610 to 0.647 (Fig. 3a4a). SVM had the highest overall accuracy (0.647) among the five models, followed closely by the accuracies of KNN (0.631) and RF (0.629). XGB (0.611) and MLP (0.610) were relatively lower among these models. The highest kappa coefficient was generated from XGB (0.240), followed by RF

(0.238), KNN (0.234) and MLP (0.230), and the worst performer was SVM, with kappa coefficient dropping to 0.186 (Fig. 3b4b).

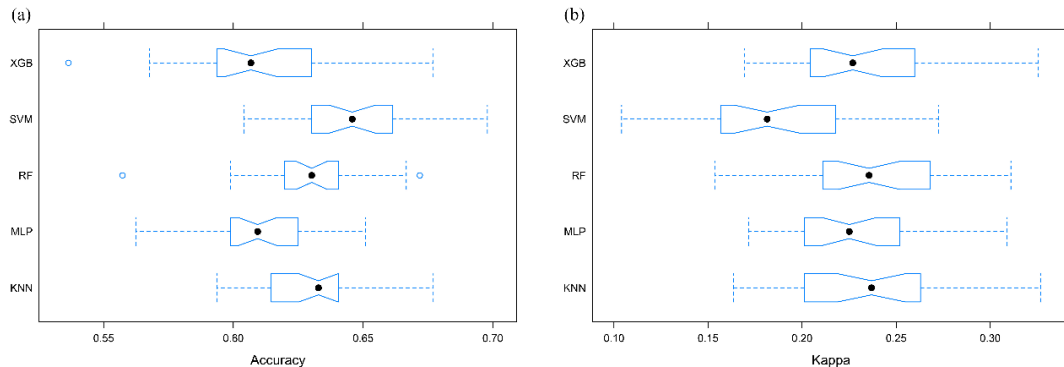


Figure 34. (a) The overall accuracies and (b) kappa coefficients for different machine learning models of KNN, MLP, RF, SVM and XGB.

The AUC with regard to each soil texture type of 640 soil sampling points predicted from five different models demonstrated that the ranking of the AUC was RF>XGB>SVM>KNN>MLP in the case of fewer soil sampling points (CILo, LoSa, Sa, SaCILo and Si). However, in the case of the types with more soil sampling points (Lo, SaLo, SiLo, SiCILo), the ROC curves exhibited roughly the same shape for each model (Fig. 45); therefore, the order of performance was as follows: RF>SVM>XGB>MLP>KNN.

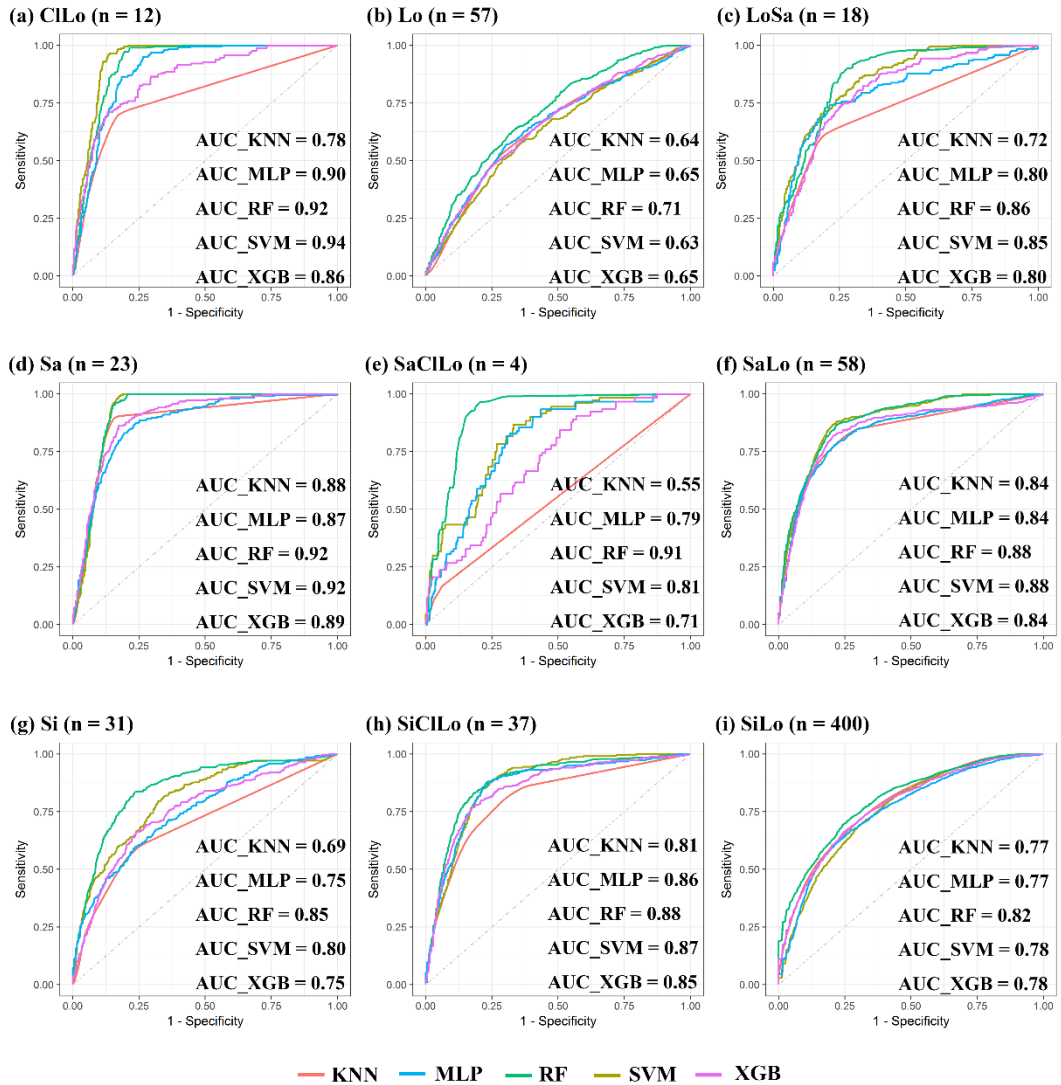


Figure 45. The AUC for different machine learning methods of each soil texture type (a) CILo (b) Lo (c) LoSa (d) Sa (e) SaCILo (f) SaLo (g) Si (h) SiCILo (i) SiLo; n was the sampling points for different soil texture types.

We combined the PRCs with five machine-learning methods to evaluate the performance of these models with respect to predicting each soil texture type using soil [psfPSF](#) imbalanced data with different samples of soil texture types (Fig. 56). We found that the AUPRC of types with fewer positive examples were typically small, especially in the case of SaCILo (only four samples), which resulted in unsatisfying consequences because the lack of soil sampling points made models learn poorly during the training process. Hence, the soil texture types (Lo, SaLo, SiLo, SiCILo) with more positive examples delivered superior results to those with fewer positive examples. Moreover, these soil texture types had significant differences in AUPRCs. For example, SiLo, which had the largest number of samples, was the most effective among these nine types. The

total AUPRC calculated by the weights of samples for AUPRC of each type was applied to evaluate the effect of each model, and the order was as follows: RF (0.646)>XGB (0.616)>KNN (0.601)>MLP (0.600)>SVM (0.599).

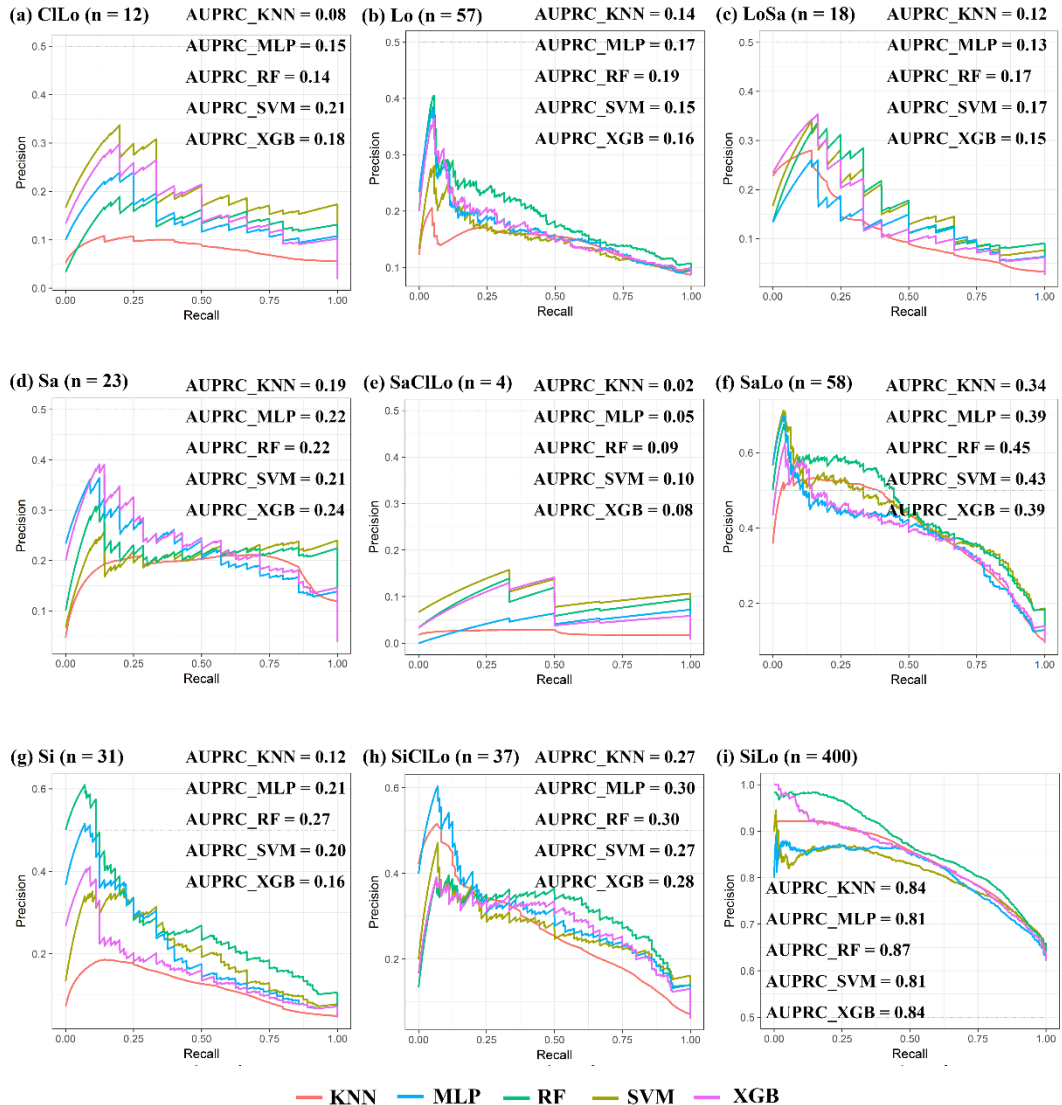


Figure 56. The AUPRC for different machine learning methods of each soil texture type (a) CILo (b) Lo (c) LoSa (d) Sa (e) SaCILo (f) SaLo (g) Si (h) SiCILo (i) SiLo; n was the sampling points for different soil texture types.

3.2.2 Comparison of the prediction maps for soil texture classification

Prediction maps of soil texture types in the HRB using machine-learning models delivered quite different spatial distributions in the overall performance of different models (Fig. 67). The abundance indices pointed out that all models could not predict

the type of SaClLo; in other words, KNN and XGB predicted 8 of 9 types, followed closely by RF (7 of 9 types) and MLP (6 of 9 types). However, SVM predicted only two types, which was an unsatisfactory result associated with the lowest kappa coefficient (Fig. 34). Additionally, the prediction effects of different models were different in the distributions of soil texture types in the HRB. The consequences of RF and XGB illustrated that the main soil texture types in the northwest of the lower reaches of HRB were mostly LoSa, while other prediction models produced SaLo. On the upper reaches of the HRB, soil texture types generated from RF were more abundant and more in accordance with the real environment.

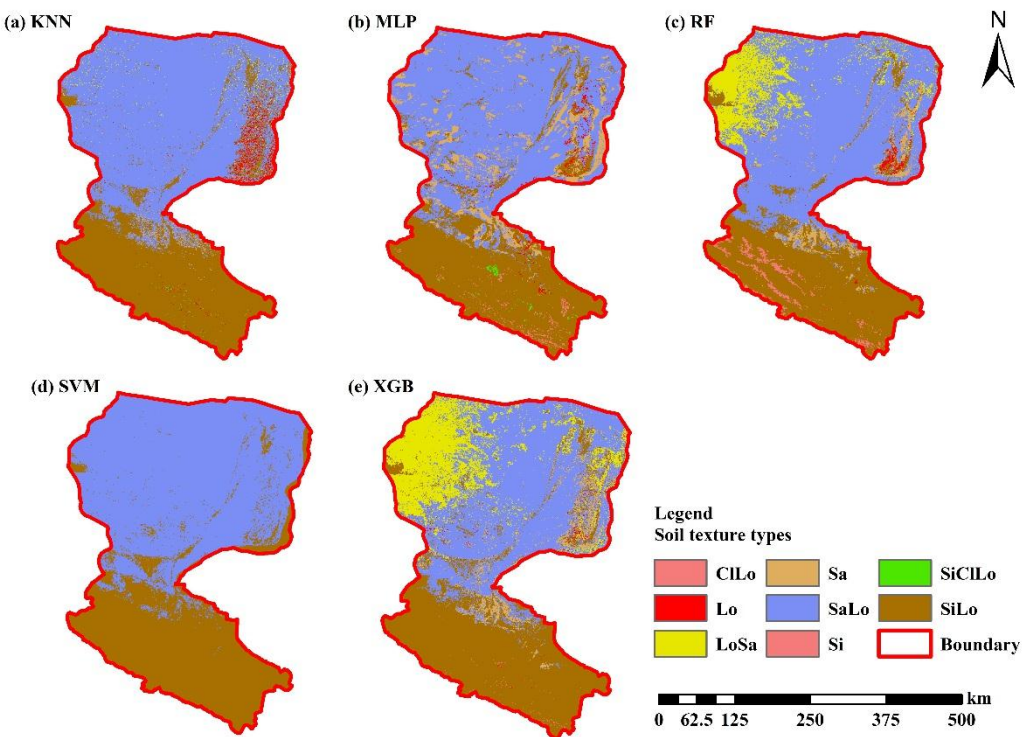


Figure 67. Soil texture classification prediction map of different soil texture types of (a) KNN, (b) MLP, (c) RF, (d) SVM and (e) XGB.

10 3.3 Comparison of the machine learning models combined with log-ratio transformed methods in the interpolation of soil psfPSF

3.3.1 Comparison of the validation indicators for interpolation of soil psfPSF

We compared the performance of each machine-learning model combined with the original (untransformed) and the log ratio transformed data of soil psfPSF. The results indicated that the accuracies of STRESS of the methods combined with log ratio transformed data were superior to other approaches using original (untransformed) data (Table 2). With respect to KNN, MLP,

RF and XGB, the RMSE, MAE, R² and AD generated from original (untransformed) data outperformed log ratio transformed data; for SVM, log ratio transformed data delivered superior improvement. For instance, SVM_CLR and SVM_ILR had higher R² and lower RMSE and MAE than SVM_ORI of sand, silt and clay.

By comparison among different log ratio transformed data of the same machine-learning model, ILR and CLR outperformed ALR in these models, other than MLP, showing a slight difference. As shown in Table 2, KNN_CLR demonstrated the most remarkable performance among the three KNN models using different log ratio transformed data with highest R² (sand: 48.48 %; silt: 38.37 %; clay: 41.43 %) and lowest RMSE (sand: 15.82 %; silt: 14.77 %; clay: 7.09 %) and MAE (sand: 11.21 %; silt: 10.74 %; clay: 5.58 %). Furthermore, CLR and ILR generated relatively similar consequences for each model of RF and SVM; with respect to XGB, XGB_ILR showed the best performance with all indicators we measured, aside from RMSE (6.75 %) and MAE (5.36 %) of clay, and STRESS (0.63).

We also compared five different machine-learning models using the same log ratio transformation approaches. In the case of ALR, ALR_RF had talent, with the lowest RMSE (sand: 15.50 %; silt: 14.43 %; clay: 6.62 %) and MAE (sand: 10.90 %; silt: 10.52 %; clay: 5.24 %), the highest R² (sand: 50.57 %; silt: 41.23 %; clay: 48.90 %), and the lowest AD (0.86) and STRESS (0.61), followed by SVM_ALR, XGB_ALR, KNN_ALR and MLP_ALR. Regarding CLR and ILR, RF also produced the most preferable performance followed by SVM, XGB, KNN and MLP. For original (untransformed) data, RF outperformed other models in accordance with log ratio approaches, and the next were XGB, SVM, KNN and MLP. Therefore, it is clear that RFs demonstrated the most extraordinary indicators of RMSE, MAE, R² and AD from the untransformed model and the best STRESS from the log ratio models (RF_ALR, RF_CLR and RF_ILR).

Table 2. The comparisons of accuracies of different machine-learning models combined with original (untransformed) and transformed data.

	RMSE (%)			MAE (%)			R ² (%)			AD	STRESS
	Sand	Silt	Clay	Sand	Silt	Clay	Sand	Silt	Clay		
KNN_ALR	16.05	15.04	7.12	11.35	10.93	5.59	47.02	36.11	41.07	0.90	0.62
KNN_CLR	15.82	14.77	7.09	11.21	10.74	5.58	48.48	38.37	41.43	0.88	0.62
KNN_ILR	15.82	14.82	7.14	11.22	10.84	5.60	48.46	37.88	40.74	0.88	0.64
KNN_ORI	15.51	14.47	7.05	11.12	10.51	5.49	50.59	40.92	42.24	0.84	0.66
MLP_ALR	15.83	15.07	7.43	11.42	11.06	5.97	48.50	35.82	35.79	0.92	0.66
MLP_CLR	15.84	15.07	7.41	11.45	11.05	5.96	48.42	35.86	36.19	0.92	0.66
MLP_ILR	15.84	15.07	7.40	11.46	11.04	5.95	48.40	35.85	36.32	0.92	0.66
MLP_ORI	15.80	14.72	6.96	11.50	10.85	5.52	48.75	38.84	43.72	0.90	0.68
RF_ALR	15.50	14.43	6.62	10.90	10.52	5.24	50.57	41.23	48.90	0.86	0.61
RF_CLR	15.28	14.22	6.61	10.70	10.25	5.21	51.95	42.89	49.16	0.86	0.61
RF_ILR	15.27	14.25	6.66	10.66	10.26	5.26	51.99	42.60	48.28	0.86	0.61
RF_ORI	15.09	13.86	6.31	10.65	9.99	5.00	53.28	45.77	53.75	0.84	0.66
SVM_ALR	15.66	14.59	6.76	11.66	10.88	5.34	49.61	39.87	46.89	0.88	0.66
SVM_CLR	15.27	14.36	6.87	11.01	10.41	5.41	52.12	41.85	45.14	0.87	0.65
SVM_ILR	15.29	14.37	6.84	10.92	10.43	5.42	51.99	41.69	45.58	0.87	0.65
SVM_ORI	15.30	14.38	6.92	10.94	10.32	5.43	51.98	41.71	44.45	0.87	0.67
XGB_ALR	15.82	14.92	6.72	11.32	11.01	5.35	48.57	37.23	47.44	0.88	0.64
XGB_CLR	15.70	14.80	6.75	10.96	10.67	5.39	49.23	38.10	46.90	0.88	0.62
XGB_ILR	15.45	14.57	6.75	10.91	10.52	5.36	50.88	40.01	47.01	0.88	0.63
XGB_ORI	15.15	14.05	6.47	10.88	10.15	5.15	52.85	44.27	51.36	0.86	0.68

3.3.2 Comparison of the interpolation maps of soil ~~psfPSF~~

Interpolation maps of soil ~~psfPSF~~ (sand, silt and clay) using log ratio transformed data (ILR) and original (untransformed) data were represented in Figs. 78, S1 and S2. At first glance, there was a negligible difference between ILR and ORI based on the same machine-learning model. However, the maps generated from models combined with ILR transformed data showed closer ranges to the original soil sampling data in the case of sand (0.98—99.66 %), silt (0.17—95.87 %) and clay (0.03—39.77 %), and the texture features were more suitable for the distributions of the real environment (Figs. 78, S1 and S2). With respect to different machine-learning models, RF and XGB delivered [prediction maps that were closer to the range of the distribution of original data](#)[more detailed information about texture features in prediction maps](#) than did KNN, SVM and MLP.

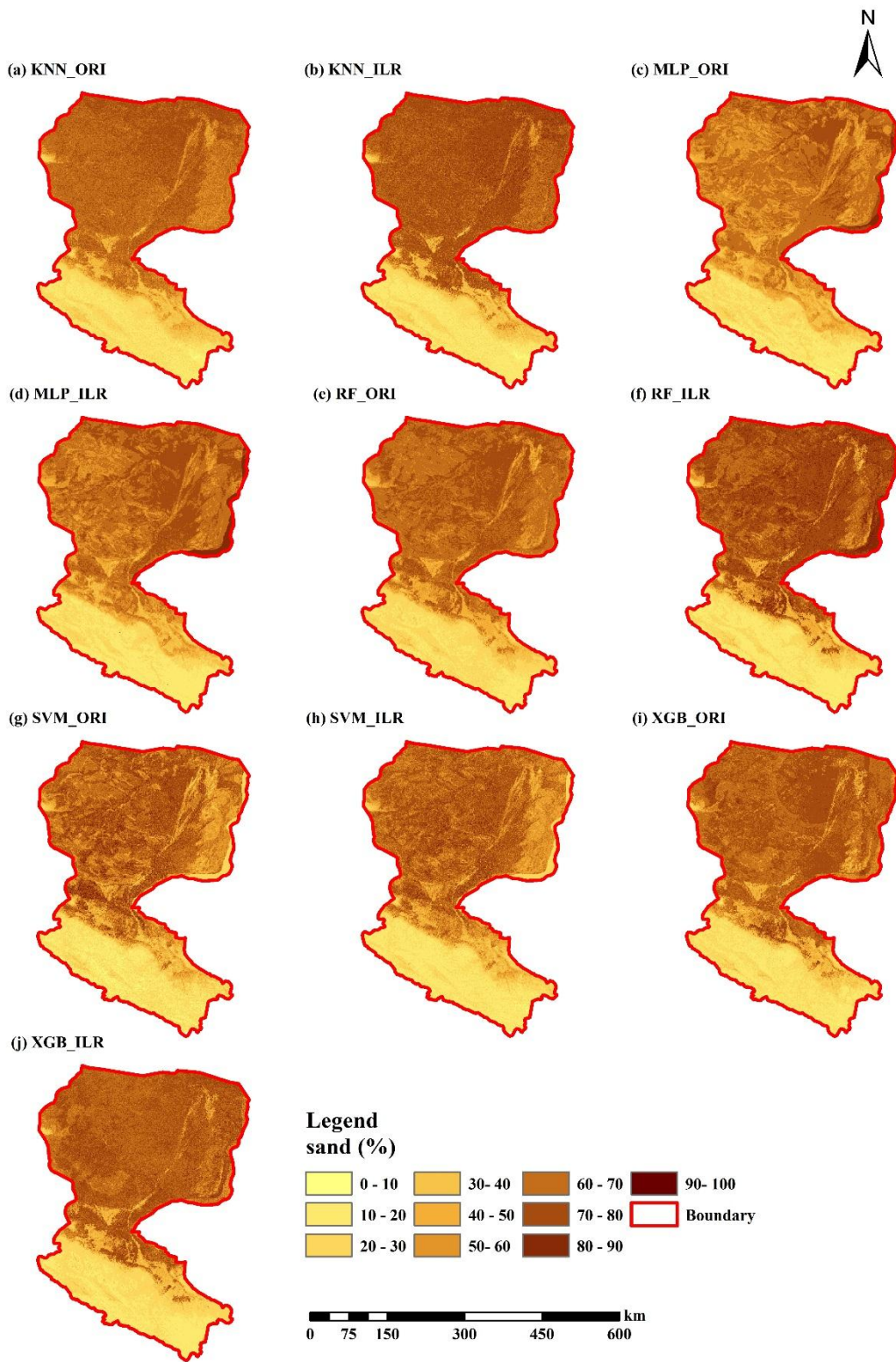


Figure 78. The interpolation maps of sand fraction. [All the ranges of prediction maps of sand \(approximately 9.0—90.0 %\) were within the range of the original data \(0.98—99.66 %\). RF_ILR \(7.9—94.7 %\) and XGB_ORI \(1.8—92.4 %\) generated wider output distributions and were relatively closer to the range of the distribution of original data than other prediction maps such as KNN_ILR \(7.3—88.6 %\), KNN_ORI \(7.8—80.8 %\), MLP_ILR \(8.8—90.8 %\), MLP_ORI \(9.0—90.3 %\), RF_ORI \(9.0—81.0 %\), SVM_ILR \(6.5—85.6 %\), SVM_ORI \(7.3—90.0 %\) and XGB_ILR \(5.0—88.5 %\).](#)

5

3.4 Comparison of direct and indirect soil texture classification

3.4.1 Comparison of the validation indicators for direct and indirect soil texture classification

Compared with the classification performance of the five machine-learning models using original (untransformed) data, the overall accuracies and kappa coefficients of models combined using log ratio transformed data were improved, especially RF

10 and XGB, which combined with all three log ratio approaches were superior to the interpolation methods using original data.

Table 3 shows that the overall accuracy (0.631) and kappa coefficient (0.245) of the original method in KNN models were better than any other log ratio transformed methods. In summary, the ILR transformation method of five machine-learning models showed the highest overall accuracy among three log ratio transformation approaches (KNN: 0.628; MLP: 0.614; RF: 0.631; SVM: 0.631; XGB: 0.632), which also demonstrated the best performance with regard to kappa coefficients (KNN:

15 0.244; RF: 0.291; SVM: 0.239; XGB: 0.252), except for MLP (ALR: 0.216; CLR: 0.216; ILR: 0.214). We also compared direct

classification (Fig. 34) with indirect classification and found that the highest values of overall accuracy of indirect classification (KNN: 0.631; MLP: 0.614; RF: 0.628; SVM: 0.638; XGB: 0.632) were slightly decreased in comparison of direct classification (KNN: 0.631; MLP: 0.610; RF: 0.629; SVM: 0.647; XGB: 0.611) for RF and SVM, and improved or kept stable for MLP and XGB, and KNN, respectively. In turn, the kappa coefficients were greatly modified using indirect classification (KNN: 0.245;

20 MLP: 0.216; RF: 0.291; SVM: 0.239; XGB: 0.252) compared with direct classification (KNN: 0.234; MLP: 0.230; RF: 0.238;

SVM: 0.186; XGB: 0.240), other than MLP; peculiarly, RF_ILR increased the kappa coefficient to 0.291 (21.3 % improvement) while keeping accuracy stable, which showed the highest kappa coefficient among these methods.

Table 3. Overall accuracies and kappa coefficients calculated from soil texture classification by the interpolated maps from five models using original (untransformed) data and log ratio transformed data.

Methods	Overall accuracy	Kappa coefficient
KNN_ALR	0.623	0.236
KNN_CLR	0.627	0.241
KNN_ILR	0.628	0.244
KNN_ORI	0.631	0.245
MLP_ALR	0.614	0.216
MLP_CLR	0.614	0.216

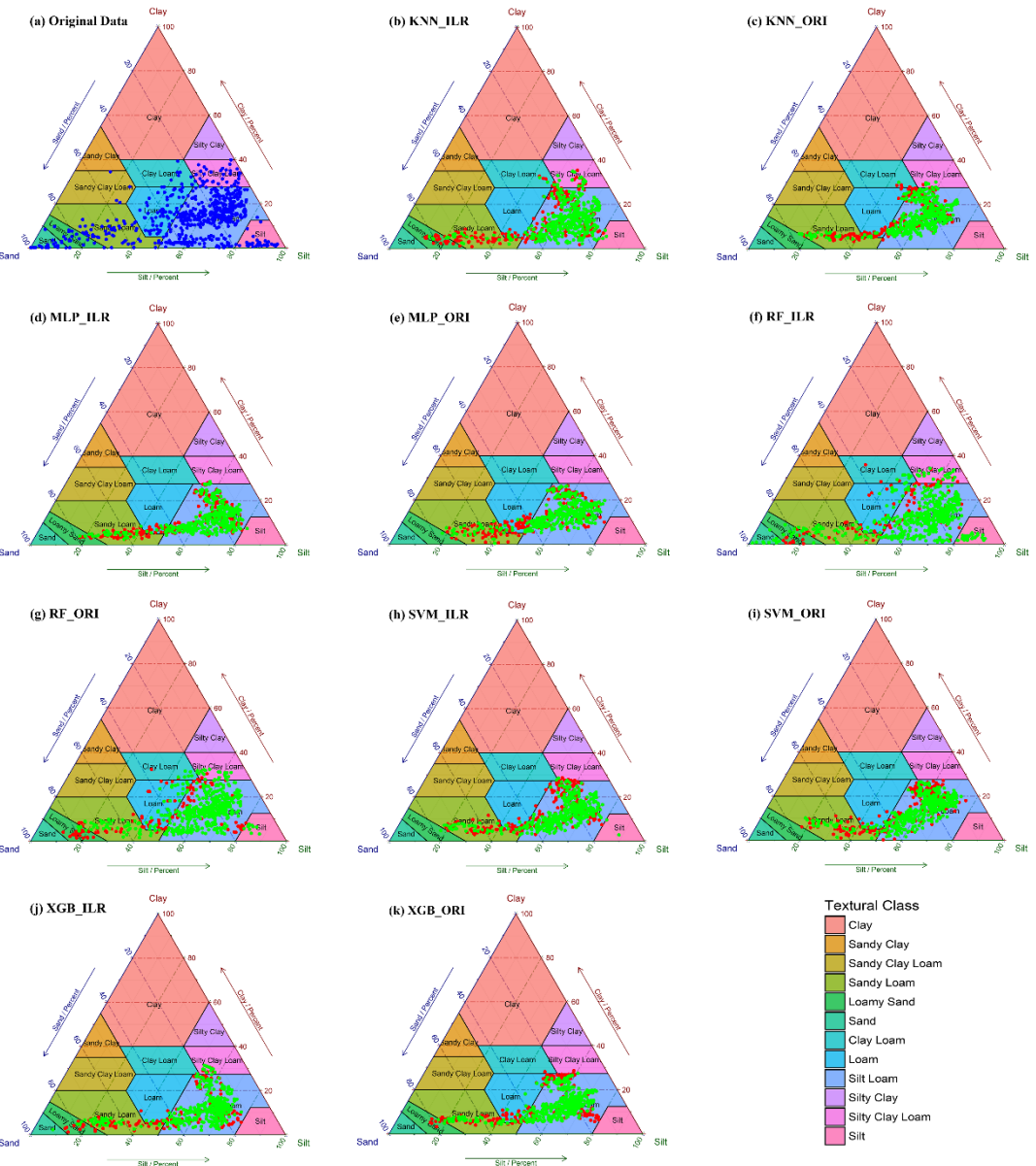
MLP_ILR	0.614	0.214
MLP_ORI	0.611	0.216
RF_ALR	0.619	0.284
RF_CLR	0.625	0.276
RF_ILR	0.628	0.291
RF_ORI	0.619	0.279
SVM_ALR	0.591	0.205
SVM_CLR	0.630	0.227
SVM_ILR	0.631	0.239
SVM_ORI	0.638	0.232
XGB_ALR	0.610	0.226
XGB_CLR	0.612	0.240
XGB_ILR	0.632	0.252
XGB_ORI	0.619	0.239

3.4.2 The prediction performance of soil texture types from different methods

The distributions of soil texture classes using original (untransformed) data and ILR transformed data are illustrated in the USDA soil texture triangle (Fig. 8g). The triangle of the original data (Fig. 8a1b) shows wider ranges of spatial dispersion than the interpolation data using machine-learning models, revealing the properties of aggregate from the sides to the center of triangles.

With respect to these machine-learning models, RF showed the most dispersed feature in accordance with the original data. The distributions predicted from models combined with ILR transformed data were more discrete and more associated with the original soil ~~psfPSF~~ data than those resulting from ORI approaches. The results of prediction represented striking differences in that the error ratio (red color) of soil sampling points on types of LoSa, SaLo and Lo (left side of triangles) were significantly more than those on types of SiLo and Si (the right side of triangles) for most models, especially KNN and MLP.

The log ratio approaches overestimated the content of silt in the process of transformation (Fig. 23); in this way, these points were biased to the right of the USDA soil texture triangle based on overall contraction (regression smoothing effects), crossing the classification boundary and becoming other soil texture types. RF_ILR (Fig. 8f9e) delivered the highest right ratio (RR) among these models, and the classification accuracy was enhanced using the ILR approach (83.9%) compared with the ORI approach (81.7%). In the case of other models, the differences between original and log ratio approaches were negligible. We also compared the RR of indirect classification models with those of direct classification, demonstrating all RRs of direct classification were higher (KNN: 67.97 %; MLP: 75.16 %; RF: 100 %; SVM: 66.09 %; XGB: 81.09 %), especially RF and XGB; however, we removed this evaluation indicator because the same data sets were employed in the processes of training and predicting.



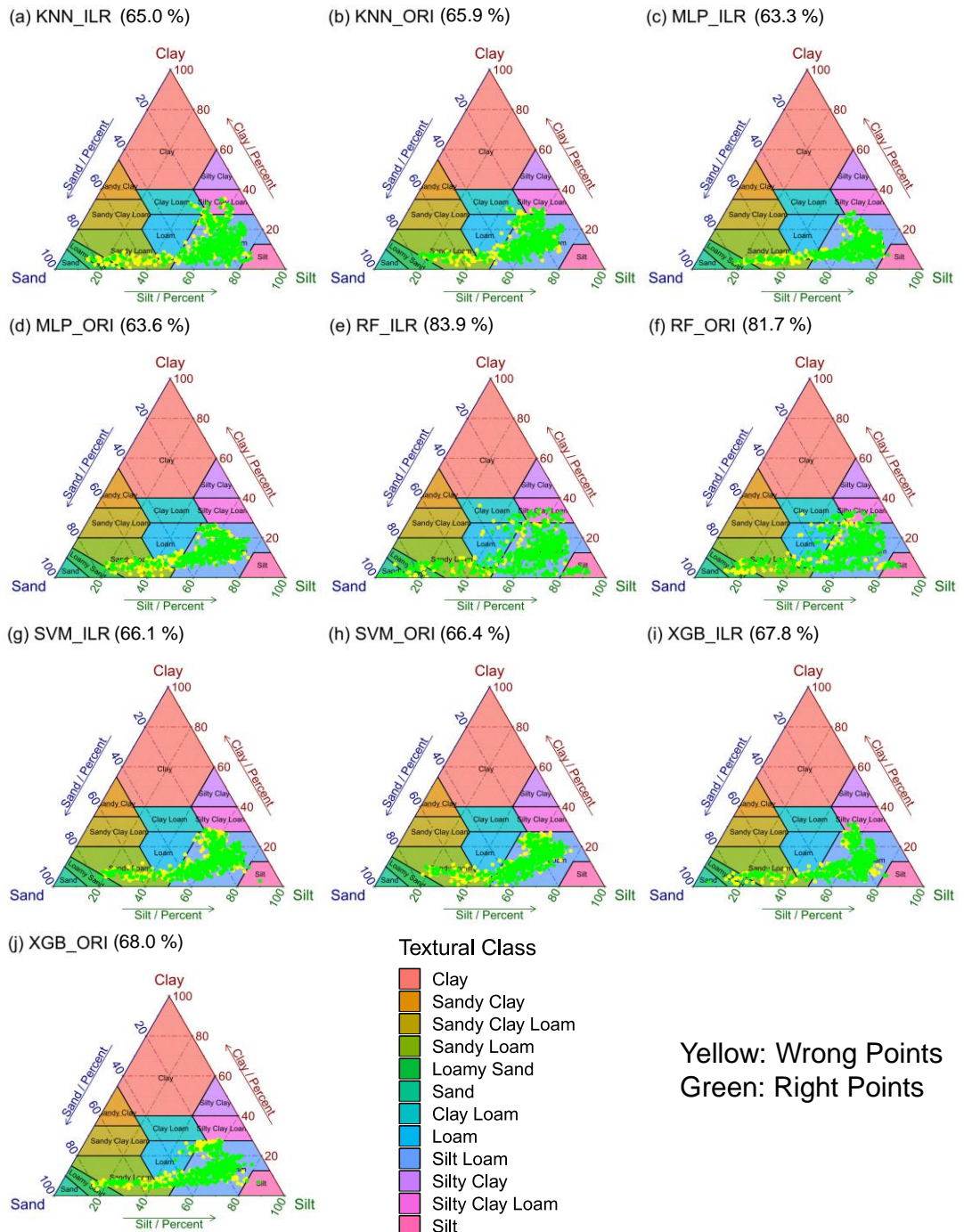


Figure 9. Soil texture types of 640 soil samples shown in USDA texture triangle. The results of soil PSF were generated from (a) KNN_ILR, (b) KNN_ORI, (c) MLP_ILR, (d) MLP_ORI, (e) RF_ILR, (f) RF_ORI, (g) SVM_ILR, (h) SVM_ORI, (i) XGB_ILR, and (j) XGB_ORI. Note that right points (green) mean that the predicted soil texture classes and these classes

corresponding to the original data were the same; wrong points (yellow) were the opposite, and the predicted right-ratios (RRs) of the soil texture types were in the bracket after interpolators in plots. **Figure 8.** Soil texture types of 640 soil samples shown in USDA texture triangle. The results of soil psfPSF were generated from (a) original (untransformed) data, (b) KNN_ILR (65.0 %), (c) KNN_ORI (65.9 %), (d) MLP_ILR (63.3 %), (e) MLP_ORI (63.6 %), (f) RF_ILR (83.9 %), (g) RF_ORI (81.7 %), (h) SVM_ILR (66.1 %), (i) SVM_ORI (66.4 %), (j) XGB_ILR (67.8 %), and (k) XGB_ORI (68.0 %). Note that the predicted right ratios (RRs) of the soil texture types were in the bracket after interpolators

3.4.3 Comparison of prediction maps of direct and indirect soil texture classification

Fig. 9–10 shows the similarity of the three log-ratio transformation methods. The soil texture maps predicted using original data is different from those generated by log-ratio transformed data, and the classification maps from the machine learning models combined the log-ratio transformed data had more detailed information. Three log-ratio transformation methods of the same machine learning model are similar in the number of each type predicted; however, there are some differences between methods using original data and those using log-ratio transformed data. All machine learning models combined with original data predicted more types of Lo and SaLo, and less types of LoSa and Si, which could also be presented in Fig. 910. The performance of different machine learning models, especially in the lower reaches of the Heihe River Basin was also compared, for log-ratio transformation methods, for KNN, KNN_ALR and KNN_CLR predicted more type of LoSa than KNN_ILR in the north of lower reaches; for each model of MLP and RF, the differences were slight; more types of Lo in the northwest of lower reaches and less LoSa near the Heihe River were generated by SVM_ALR, compared with SVM_CLR and SVM_ILR; for XGB, the performance of three maps were different due to the prediction of LoSa. We also compared the prediction of the soil texture types by direct classification (Fig. 67) with those generated by indirect classification using the same machine learning model, and found completely difference between them on the lower reaches of Heihe River Basin, such as the distribution of LoSa; on the middle and upper reaches of Heihe River Basin, all the prediction maps were similar, mainly distributed with SiLo.

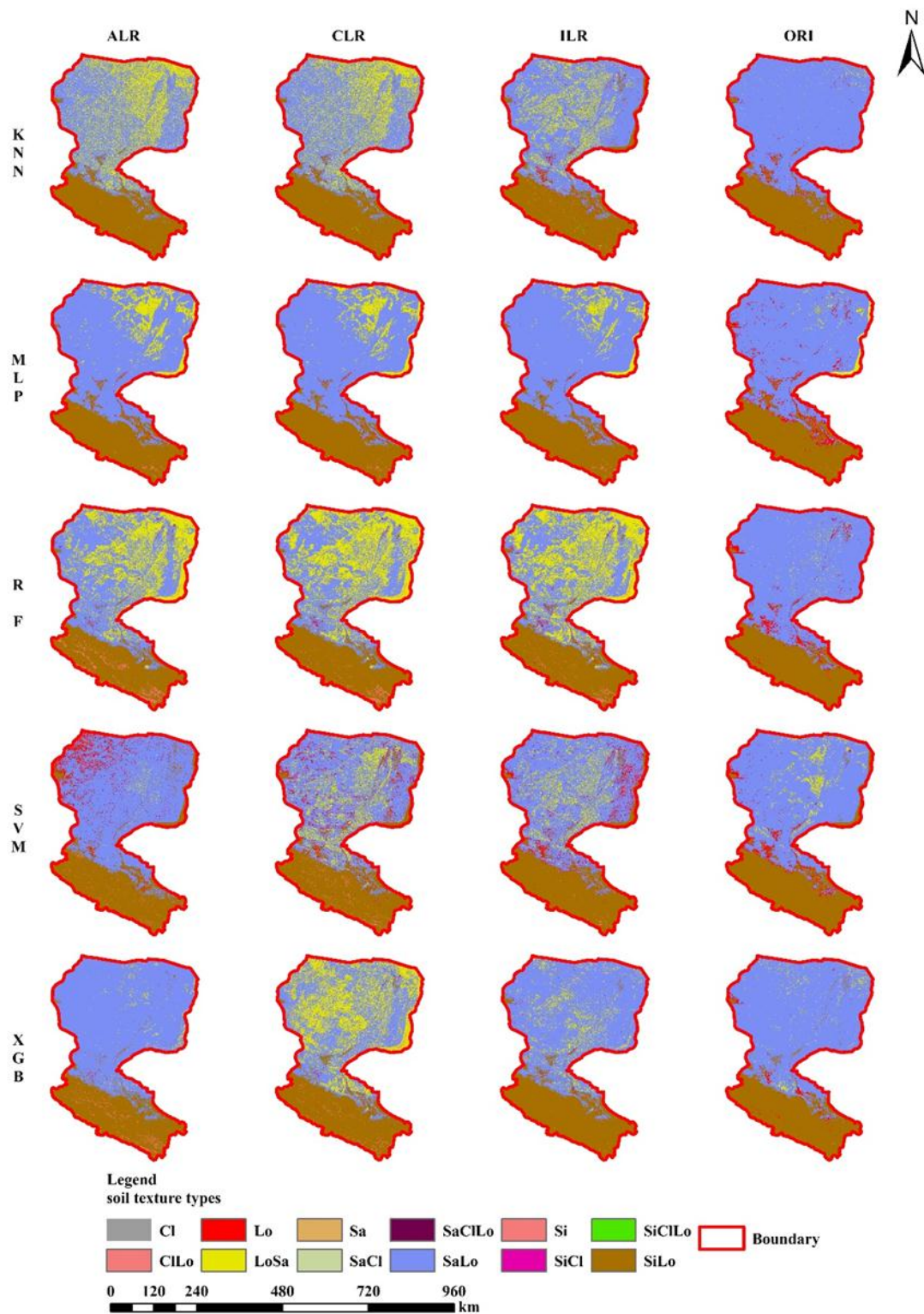
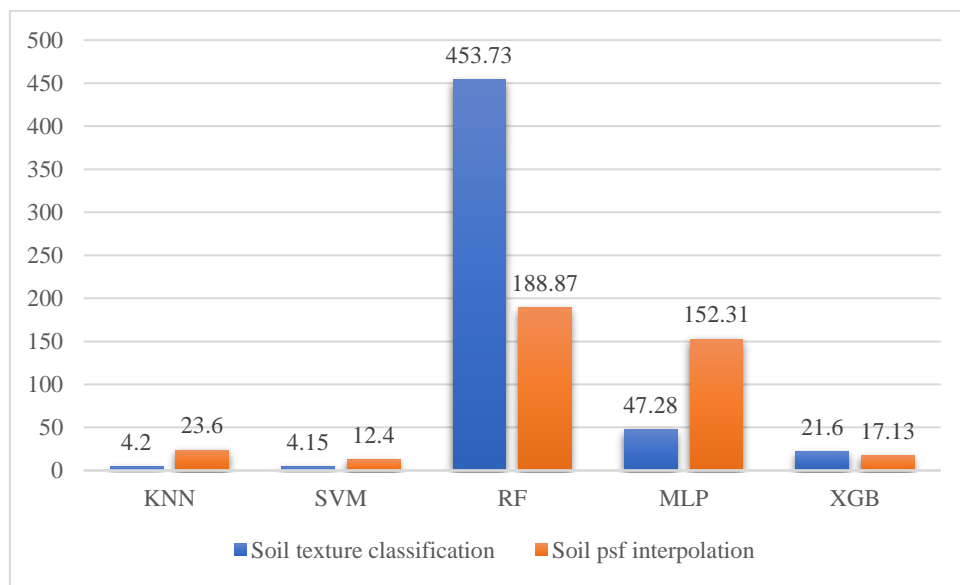


Figure 910. Soil texture classification prediction maps by soil ~~psfPSF~~ interpolation (ALR, CLR, ILR log-ratio transformation methods and the original method) of KNN, MLP, RF, SVM and XGB.

3.4.4 Comparison of ~~total computing time~~ time spending for each model in soil texture classification and soil ~~psfPSF~~ interpolation

- 5 Time spending for models was computed to compare the efficiency of different machine-learning models in soil texture classification and soil ~~psfPSF~~ interpolation (Fig. 4011). Because the differences in time spending among ORI and log ratio approaches were similar, ILR was selected for soil ~~psfPSF~~ interpolation. For the different models, RFs required the longest time for both classification (453.73 s) and regression (188.87 s), which may cause it to lose advantages when dealing with big data sets. KNN (classification: 4.2 s, regression: 23.6 s) and SVM (classification: 4.15 s, regression: 12.4 s) both showed
10 shorter time in not only classification but also regression. Likewise, XGB (classification: 21.6 s, regression: 17.13 s) was much more stable and used less time, and the data processes were simpler compared with MLP (classification: 47.28 s, regression: 152.31 s). Moreover, it delivered better performance than KNN and SVM in prediction maps of HRB, demonstrating an effective way of dealing with larger data.



- 15 **Figure 4011.** Average time spent running 30 times for KNN, MLP, RF, SVM and XGB of soil texture classification and soil ~~psfPSF~~ interpolation.

4 Discussion

4.1 The systematic comparison of the five machine learning models

As mentioned previously, we compared the performance of different machine-learning methods containing KNN, MLP, RF, SVM and XGB. The results demonstrate that SVM had the highest overall accuracy and XGB generated the highest kappa coefficient with respect to direct soil texture classification; considering the comprehensive evaluation of AUC and AUPRC, RF showed the best performance among these machine-learning models. In the case of soil ~~psfPSF~~ interpolation, the indicators of RMSE, MAE, R², AD and STRESS showed that RFs outperformed other machine-learning models, which also indicated additional information in prediction maps of sand, silt and clay and models of XGB. For the indirection classification of soil texture, the USDA soil texture triangles generated from RF were the closest to the distribution of the original data (Fig. 8a1b), with the highest classification right ratio. Prediction maps of indirect soil texture classification were also considered, demonstrating RF and MLP models were more suitable for the real environment, especially the models combined with log ratio transformation approaches. Time spending of different machine-learning models showed that KNN, SVM and XGB required less time than RF and MLP to fit large data sets.

The comparisons of machine-learning models were also mentioned in previous reports. Heung et al. (2016) demonstrated that tree learners, such as RFs, delivered better performance than KNN and SVM due to the advantages of the interpretability of the results for classification problems in soil science; tree learners (decision trees) were also shown by Taghizadeh-Mehrjardi et al. (2015), indicating that the decision trees and ANN outperformed KNN, RF and SVM. ANNs, however, were typically complicated, which was true for our study due to the standardization and back transformation of MLP. In contrast, Wu et al. (2018) proposed that SVM revealed reliable consequences in direct soil texture classification, which was quite different from our results. In general, as binary classifiers, multi-class tasks can be handled as well using SVM; however, this is no longer the case in our study, as only 2 types of soil texture were generated from SVM, showing unsatisfactory results in both kappa coefficients and prediction maps. The consequences may be explained by the imbalanced data of soil texture types. For more information about tree learners in soil science for regression, Hengl et al. (2017) found lower R² using XGB than RF on a global-scale prediction. Zeraatpisheh et al. (2018) put forward the lowest RMSE and the highest R² using RF compared with multiple linear regression and regression trees for the prediction of clay, and this conclusion was similar to our study. For the total computing time, RF revealed the longest time with respect to both classification (453.73 s) and regression (188.87 s); moreover, 1000 trees were used because of the parameter's adjustment. However, the computing time may drop significantly and accuracy do not lose much by reducing the number of trees, which need to be considered in future research.

4.2 The systematic comparison of the models combined with three log-ratio transformed data and original data

We compared the performance of models combined with three types of log ratio transformed data and original (untransformed) data for soil ~~psfPSF~~ interpolation and indirect soil texture classification, and the results showed that the models using original

data performed better in the case of indicators, such as RMSE, MAE, R^2 and AD, while the models using log ratio transformed data improved the STRESS. The interpolation maps of soil **psfPSF** using the ILR approach illustrated closer ranges of soil sampling data than those based on the ORI approach. With respect to the indirect soil texture classification, models using log ratio transformed data improved the overall accuracies and kappa coefficients, such as RF and XGB. The USDA soil texture triangles showed more discrete distribution and more accordance with soil sampling data using the ILR transformation method. Better performance was shown in soil texture classification prediction maps generated from log ratio transformed data. Among the three log ratio approaches, ILR and CLR were superior to ALR for the reason of more accurate indicators of soil **psfPSF** interpolation and indirect soil texture classification, as well the performance of prediction maps. Additionally, log ratio approaches modified soil sampling data to become more symmetric (Filzmoser et al., 2009); however, this improvement was not greatly effective [because of outliers, in order to show the true environmental distribution, we did not remove these outliers](#). Fig.[2-3](#) illustrated that soil sampling data for sand and clay were right-skewed, and silt was left-skewed because the silt component was predominant. The ALR transformed method enhanced soil sampling data of sand; nevertheless, the ALR_sand was still right-skewed, similar to the CLR_sand, presenting the lack of adjustment. In contrast, the ILR_sand changed from right-skewed to left-skewed; from this point of view, the over-adjustment was revealed. Similarly, the lack of adjustments was also shown in CLR_silt and ILR_silt; over-adjustments included ALR_silt, ALR_clay, CLR_clay and ILR_clay, making images that were different from normal distribution, and the p values of k-s tests were not significant. In our previous research (Wang and Shi, 2017), the ILR approach had better performance than ALR and CLR, with the highest R^2 and lowest AD. The CLR approach also performed well due to the lowest RMSE and mean error (ME) among the three log ratio approaches. When comparing the original (untransformed) and log ratio approaches, kriging approaches based on the log ratio delivered slightly decreased accuracies, which was similar to the conclusion in our study.

4.3 The systematic comparison of the direct and indirect classification for soil **psfPSF**

Indirect classification showed not only better performance with respect to accuracy evaluation but also more accordance with the real environment than direct classification. The highest kappa coefficient generated from indirect classification (RF_ILR: 0.291) demonstrated obvious improvement (approximately 21.3 %) compared with that of direct classification (XGB: 0.240), keeping the highest overall accuracy stable (-1.4 %) at the same time (direct: 0.647; indirect: 0.638, respectively).

Compared with the real soil texture distribution and environment of the HRB, SiLo overlaid the upper reaches of HRB, and SaLo and Lo were in the south of the upper reaches of HRB showed strip distribution. Moreover, an uncovered area was detected in the northwest of the lower reaches of HRB, where it cannot be predicted due to a lack of information (soil samples) input in the process of model training. The main soil texture types of the lower reaches of the HRB were SiLo, LoSa and small amounts of SaLo and Lo distributed in uncovered area. The main soil texture types predicted by direct classification using machine-learning models were SaLo and SiLo; RF and XGB delivered much more LoSa than other direct classification models. However, all these models predicted that the main soil type of the lower reaches of HRB was SaLo, which was not fitted for

the real environment (LoSa). In fact, LoSa and SaLo were obviously most confused classes; however, they are fairly similar to each other (see Fig. 1 or Fig. 89). In addition, because of the limitation of the train sets, direct classification can only predict types in the training data; in contrast, indirect classification broke such limitations, and new prediction types arose due to the transformation from soil ~~psfPSF~~ to soil texture types. Moreover, more suitable matching performance with the real environment
5 should be considered, such as the log ratio approaches of MLP, RF, KNN_ALR, KNN_ILR and XGB_CLR. The direct soil texture classification generated relative unsatisfactory consequences. Although the indirect soil texture classification outperformed the direct one, kappa coefficients for indirect classification at fair-level (0.21—0.40) also need to be enhanced. Hence, soil sampling data appear to be comprehensively meaningful, considering accuracy improvement. In the case of soil sampling data, the laser diffraction approach we mentioned above was applied to obtain the discrete representation of particle
10 size curves based on the given quantiles of these curves, i.e., soil particle size fractions (~~psfPSF~~, sand, silt and clay). Subsequently, soil ~~psfPSF~~ data were separately modeled for prediction and validation. Another perspective of soil ~~psfPSF~~ should be considered, i.e., the probability density functions of particle size curves (so-called functional compositions), which are non-negative values that integrate to 1 (or 100 %) and can be considered as compositional data with infinitesimal parts
15 (Menafoglio et al., 2014). Unlike conventional approaches, the viewpoints of functional compositions are beneficial to acquiring complete and continuous information rather than discrete information (sand, silt and clay) and soil texture and soil particle size fractions can be extracted using the stochastic simulation of soil particle-size curves (Menafoglio et al., 2016b). Previous studies applied such functional-compositional data for the simulation of particle size curves combined with geostatistical or machine-learning methods such as kriging and bayes approaches (Menafoglio et al., 2016a) in hydrogeology,
20 demonstrating more remarkable results compared with traditional methods. Therefore, which data should be used is the key points of accuracy improvement in future research.

5 Conclusion

We systematically compared a total of 45 models for direct and indirect soil texture classification, and soil ~~psfPSF~~ interpolation using five machine-learning approaches combined with original (untransformed) and three different log ratio transformed data in the HRB. The results indicate that as flexible and stable models, tree learners such as RF delivered powerful performance
25 in both classification and regression and were superior to other machine-learning models mentioned above. As a new and sub-optimal machine-learning method in soil science, XGB appeared to be more meaningful and more computationally efficient when dealing with large data sets. In addition, the log ratio approaches had advantages of modifying STRESS in soil ~~psfPSF~~ interpolation. Moreover, the indirect soil texture classification outperformed the direct one, especially when combined with the log ratio approaches. The indirect soil texture classification generated preferable consequences in both cases of accuracy indicators and prediction maps. More appropriate environmental covariates and interpolation techniques, [more efficient soil PSF data transformation methods](#)[more symmetric distribution of soil sampling data](#) (or multiple perspectives of compositional

data selection), and systematic parameter adjustment algorithms of compositional data are key to improving accuracy in the future.

- 5 *Data availability.* The soil sampling data is provided by “Cold and Arid Regions Science Data Center at Lanzhou” (<http://westdc.westgis.ac.cn>; <http://westdc.westgis.ac.cn/DOI:10.3972/heihe.009.2013.db>; <http://westdc.westgis.ac.cn/DOI:10.3972/heihe.009.2013.db>; <http://westdc.westgis.ac.cn/DOI:10.3972/heihe.00135.2016.db>; <http://westdc.westgis.ac.cn/DOI:10.3972/hiwater.147.2013.db>; <http://westdc.westgis.ac.cn/DOI:10.3972/heihe.037.2014.db>; <http://westdc.westgis.ac.cn/DOI:doi:10.3972/heihe.0034.2013.db>);
- 10 <http://westdc.westgis.ac.cn/DOI:10.3972/heihe.093.2013.db>) and part of environmental covariates data can be accessed through <http://westdc.westgis.ac.cn/> (last access: 29 October 2018). The meteorological data can be accessed through <http://data.cma.cn/> (last access: 29 October 2018).
- 15 *Author contributions.* WS contributed to soil data sampling, oversaw the design of the entire project. MZ performed the analysis and wrote the manuscript. Both authors contributed to writing this paper and interpreting data.

Competing interests. The authors declare that they have no conflict of interest.

20

Acknowledgements. This study was supported by the National Natural Science Foundation of China (Grant No. 41771111 and 41771364), Fund for Excellent Young Talents in Institute of Geographic Sciences and Natural Resources Research, Chinese Academy of Sciences (2016RC201), and the Youth Innovation Promotion Association, CAS (No. 2018071).

25 **References**

- Abdi, D., Cade-Menun, B. J., Ziadi, N., and Parent, L.-E.: Compositional statistical analysis of soil p-31-nmr forms, Geoderma, 257, 40-47, <https://doi.org/10.1016/j.geoderma.2015.03.019>, 2015.
- Adhikari, K., and Hartemink, A. E.: Linking soils to ecosystem services - a global review, Geoderma, 262, 101-111, <https://doi.org/10.1016/j.geoderma.2015.08.009>, 2016.
- 30 Aitchison, J.: The statistical-analysis of compositional data, Journal of the Royal Statistical Society Series B-Methodological, 44, 139-177, 1982.

- Aitchison, J.: On criteria for measures of compositional difference, Mathematical Geology, 24, 365-379, <https://doi.org/10.1007/bf00891269>, 1992.
- Bacon-Shone, J. H.: A short history of compositional data analysis, in: Compositional data analysis: Theory and applications, Wiley, Chichester, West Sussex, 3, 2011.
- 5 Bagheri Bodaghabadi, M., Antonio Martinez-Casasnovas, J., Salehi, M. H., Mohammadi, J., Esfandiarpoor Borujeni, I., Toomanian, N., and Gandomkar, A.: Digital soil mapping using artificial neural networks and terrain-related attributes, Pedosphere, 25, 580-591, [https://doi.org/10.1016/s1002-0160\(15\)30038-2](https://doi.org/10.1016/s1002-0160(15)30038-2), 2015.
- Bationo, A., Kihara, J., Vanlauwe, B., Waswa, B., and Kimetu, J.: Soil organic carbon dynamics, functions and management in west african agro-ecosystems, Agricultural Systems, 94, 13-25, <https://doi.org/10.1016/j.aghsy.2005.08.011>, 2007.
- 10 Behrens, T., and Scholten, T.: Chapter 25 a comparison of data-mining techniques in predictive soil mapping, in: Developments in soil science, edited by: Lagacherie, P., McBratney, A. B., and Voltz, M., Elsevier, 353-617, 2006.
- Bergmeir, C., and Benitez, J. M.: Neural networks in R using the stuttgart neural network simulator: RSNNs, Journal of Statistical Software, 46, 1-26, 2012.
- Breiman, L.: Bagging predictors, Machine Learning, 24, 123-140, <https://doi.org/10.1023/a:1018054314350>, 1996.
- 15 Breiman, L.: Random forests, Machine Learning, 45, 5-32, <https://doi.org/10.1023/a:1010933404324>, 2001.
- Brown, D. J., Clayton, M. K., and McSweeney, K.: Potential terrain controls on soil color, texture contrast and grain-size deposition for the original catena landscape in uganda, Geoderma, 122, 51-72, <https://doi.org/10.1016/j.geoderma.2003.12.004>, 2004.
- 20 Brus, D. J., Kempen, B., and Heuvelink, G. B. M.: Sampling for validation of digital soil maps, European Journal of Soil Science, 62, 394-407, <https://doi.org/10.1111/j.1365-2389.2011.01364.x>, 2011.
- Burges, C. J. C.: A tutorial on support vector machines for pattern recognition, Data Mining and Knowledge Discovery, 2, 121-167, <https://doi.org/10.1023/a:1009715923555>, 1998.
- 25 Camera, C., Zomeni, Z., Noller, J. S., Zissimos, A. M., Christoforou, I. C., and Bruggeman, A.: A high resolution map of soil types and physical properties for cyprus: A digital soil mapping optimization, Geoderma, 285, 35-49, <https://doi.org/10.1016/j.geoderma.2016.09.019>, 2017.
- Chen, T., and Guestrin, C.: Xgboost: A scalable tree boosting system, Proceedings of the 22nd ACM SIGKDD International Conference on Knowledge Discovery and Data Mining, San Francisco, California, USA, 2016.
- Chen, T., He, T., Benesty, M., Khotilovich, V., Tang, Y., Cho, H., Chen, K., Mitchell, R., Cano, I., Zhou, T., Li, M., Xie, J., Lin, M., Geng, Y., and Li, Y.: Xgboost: Extreme gradient boosting, R package version 0.71.2, available at: <https://CRAN.R-project.org/package=xgboost> (last access: 18 November 2018), 2018.
- 30 Conrad, O., Bechtel, B., Bock, M., Dietrich, H., Fischer, E., Gerlitz, L., Wehberg, J., Wichmann, V., and Böhner, J.: System for automated geoscientific analyses (saga) v. 2.1.4, Geosci. Model Dev., 8, 1991-2007, <https://doi.org/10.5194/gmd-8-1991-2015>, 2015.

- Cortes, C., and Vapnik, V.: Support-vector networks, Machine Learning, 20, 273-297,
<https://doi.org/10.1023/a:1022627411411>, 1995.
- Cover, T. M., and Hart, P. E.: Nearest neighbor pattern classification, Ieee Transactions on Information Theory, 13, 21,
<https://doi.org/10.1109/tit.1967.1053964>, 1967.
- 5 Crouvi, O., Pelletier, J. D., and Rasmussen, C.: Predicting the thickness and aeolian fraction of soils in upland watersheds of the mojave desert, Geoderma, 195, 94-110, <https://doi.org/10.1016/j.geoderma.2012.11.015>, 2013.
- Davis, J., and Goadrich, M.: The relationship between precision-recall and roc curves, Proceedings of the 23rd international conference on Machine learning, Pittsburgh, Pennsylvania, USA, 2006.
- Egozcue, J. J., Pawlowsky-Glahn, V., Mateu-Figueras, G., and Barcelo-Vidal, C.: Isometric logratio transformations for 10 compositional data analysis, Mathematical Geology, 35, 279-300, <https://doi.org/10.1023/a:1023818214614>, 2003.
- Elith, J., Leathwick, J. R., and Hastie, T.: A working guide to boosted regression trees, Journal of Animal Ecology, 77, 802-813, <https://doi.org/10.1111/j.1365-2656.2008.01390.x>, 2008.
- Fan, J., Wang, X., Wu, L., Zhou, H., Zhang, F., Yu, X., Lu, X., and Xiang, Y.: Comparison of support vector machine and 15 extreme gradient boosting for predicting daily global solar radiation using temperature and precipitation in humid subtropical climates: A case study in china, Energy Conversion and Management, 164, 102-111, <https://doi.org/10.1016/j.enconman.2018.02.087>, 2018.
- Fawcett, T.: An introduction to roc analysis, Pattern Recognition Letters, 27, 861-874,
<https://doi.org/10.1016/j.patrec.2005.10.010>, 2006.
- Filzmoser, P., Hron, K., and Reimann, C.: Univariate statistical analysis of environmental (compositional) data: Problems 20 and possibilities, Science of the Total Environment, 407, 6100-6108, <https://doi.org/10.1016/j.scitotenv.2009.08.008>, 2009.
- Follain, S., Minasny, B., McBratney, A. B., and Walter, C.: Simulation of soil thickness evolution in a complex agricultural landscape at fine spatial and temporal scales, Geoderma, 133, 71-86, <https://doi.org/10.1016/j.geoderma.2006.03.038>, 2006.
- 25 Fu, G.-H., Xu, F., Zhang, B.-Y., and Yi, L.-Z.: Stable variable selection of class-imbalanced data with precision-recall criterion, Chemometrics and Intelligent Laboratory Systems, 171, 241-250,
<https://doi.org/10.1016/j.chemolab.2017.10.015>, 2017.
Gaurang, P., Ganatra, A., Kosta, Y., and Panchal, D.: Behaviour Analysis of Multilayer Perceptronwith Multiple Hidden
Neurons and Hidden Layers, 332-337 pp., 2011.
- 30 Gobin, A., Campling, P., and Feyen, J.: Soil-landscape modelling to quantify spatial variability of soil texture, Physics and Chemistry of the Earth Part B-Hydrology Oceans and Atmosphere, 26, 41-45, [https://doi.org/10.1016/s1464-1909\(01\)85012-7](https://doi.org/10.1016/s1464-1909(01)85012-7), 2001.

- Gochis, D. J., Vivoni, E. R., and Watts, C. J.: The impact of soil depth on land surface energy and water fluxes in the north american monsoon region, Journal of Arid Environments, 74, 564-571, <https://doi.org/10.1016/j.jaridenv.2009.11.002>, 2010.
- Hengl, T., Heuvelink, G. B. M., Kempen, B., Leenaars, J. G. B., Walsh, M. G., Shepherd, K. D., Sila, A., MacMillan, R. A.,
5 de Jesus, J. M., Tamene, L., and Tondoh, J. E.: Mapping soil properties of africa at 250 m resolution: Random forests significantly improve current predictions, Plos One, 10, <https://doi.org/10.1371/journal.pone.0125814>, 2015.
- Hengl, T., de Jesus, J. M., Heuvelink, G. B. M., Gonzalez, M. R., Kilibarda, M., Blagotic, A., Shangguan, W., Wright, M. N.,
10 Geng, X., Bauer-Marschallinger, B., Guevara, M. A., Vargas, R., MacMillan, R. A., Batjes, N. H., Leenaars, J. G. B., Ribeiro, E., Wheeler, I., Mantel, S., and Kempen, B.: Soilgrids250m: Global gridded soil information based on machine learning, Plos One, 12, <https://doi.org/10.1371/journal.pone.0169748>, 2017.
- [Hengl, T., Nussbaum, M., Wright, M. N., Heuvelink, G. B. M., and Graler, B.: Random forest as a generic framework for predictive modeling of spatial and spatio-temporal variables, PeerJ, 6, 49, 10.7717/peerj.5518, 2018.](#)
- Heung, B., Ho, H. C., Zhang, J., Knudby, A., Bulmer, C. E., and Schmidt, M. G.: An overview and comparison of machine-learning techniques for classification purposes in digital soil mapping, Geoderma, 265, 62-77,
15 <https://doi.org/10.1016/j.geoderma.2015.11.014>, 2016.
- Huang, J., Subasinghe, R., and Triantafilis, J.: Mapping particle-size fractions as a composition using additive log-ratio transformation and ancillary data, Soil Science Society of America Journal, 78, 1967-1976,
<https://doi.org/10.2136/sssaj2014.05.0215>, 2014.
- Huete, A., Didan, K., Miura, T., Rodriguez, E. P., Gao, X., and Ferreira, L. G.: Overview of the radiometric and biophysical
20 performance of the modis vegetation indices, Remote Sensing of Environment, 83, 195-213,
[https://doi.org/10.1016/s0034-4257\(02\)00096-2](https://doi.org/10.1016/s0034-4257(02)00096-2), 2002.
- Huete, A. R.: A soil-adjusted vegetation index (savi), Remote Sensing of Environment, 25, 295-309,
[https://doi.org/10.1016/0034-4257\(88\)90106-x](https://doi.org/10.1016/0034-4257(88)90106-x), 1988.
- Jafari, A., Khademi, H., Finke, P. A., Van de Wauw, J., and Ayoubi, S.: Spatial prediction of soil great groups by boosted
25 regression trees using a limited point dataset in an arid region, southeastern iran, Geoderma, 232, 148-163,
<https://doi.org/10.1016/j.geoderma.2014.04.029>, 2014.
- Krasilnikov, P. V., Garcia-Calderon, N. E., Ibanez-Huerta, A., Bazan-Mateos, M., and Hernandez-Santana, J. R.: Soilscapes
in the dynamic tropical environments: The case of sierra madre del sur, Geomorphology, 135, 262-270,
<https://doi.org/10.1016/j.geomorph.2011.02.013>, 2011.
- 30 Kuhn, M.: Caret: Classification and regression training, R package version 6.0-80, available at: <https://CRAN.R-project.org/package=caret> (last access: 18 November 2018), 2018.
- Landis, J. R., and Koch, G. G.: Measurement of observer agreement for categorical data, Biometrics, 33, 159-174,
<https://doi.org/10.2307/2529310>, 1977.

- Lark, R. M., and Bishop, T. F. A.: Cokriging particle size fractions of the soil, European Journal of Soil Science, 58, 763-774, <https://doi.org/10.1111/j.1365-2389.2006.00866.x>, 2007.
- Liaw, A., and Wiener, M.: Classification and regression by randomforest, R News, 2, 18-22, 2002.
- Liess, M., Glaser, B., and Huwe, B.: Uncertainty in the spatial prediction of soil texture comparison of regression tree and
5 random forest models, Geoderma, 170, 70-79, <https://doi.org/10.1016/j.geoderma.2011.10.010>, 2012.
- ~~Marchetti, A., Piccini, C., Santucci, S., Chiuchiarelli, I., and Francaviglia, R.: Simulation of soil types in teramo province (central italy) with terrain parameters and remote sensing data, Catena, 85, 267-273, https://doi.org/10.1016/j.catena.2011.01.012, 2011.~~
- Martin-Fernandez, J. A., Olea-Meneses, R. A., and Pawlowsky-Glahn, V.: Criteria to compare estimation methods of
10 regionalized compositions, Mathematical Geology, 33, 889-909, <https://doi.org/10.1023/a:1012293922142>, 2001.
- McBratney, A. B., Santos, M. L. M., and Minasny, B.: On digital soil mapping, Geoderma, 117, 3-52,
[https://doi.org/10.1016/s0016-7061\(03\)00223-4](https://doi.org/10.1016/s0016-7061(03)00223-4), 2003.
- McNamara, J. P., Chandler, D., Seyfried, M., and Achet, S.: Soil moisture states, lateral flow, and streamflow generation in a semi-arid, snowmelt-driven catchment, Hydrological Processes, 19, 4023-4038, <https://doi.org/10.1002/hyp.5869>, 2005.
- 15 Menafoglio, A., Guadagnini, A., and Secchi, P.: A kriging approach based on aitchison geometry for the characterization of particle-size curves in heterogeneous aquifers, Stoch. Environ. Res. Risk Assess., 28, 1835-1851,
<https://doi.org/10.1007/s00477-014-0849-8>, 2014.
- Menafoglio, A., Guadagnini, A., and Secchi, P.: Stochastic simulation of soil particle-size curves in heterogeneous aquifer systems through a bayes space approach, Water Resources Research, 52, 5708-5726, 10.1002/2015wr018369, 2016a.
- 20 Menafoglio, A., Secchi, P., and Guadagnini, A.: A class-kriging predictor for functional compositions with application to particle-size curves in heterogeneous aquifers, Math Geosci., 48, 463-485, <https://doi.org/10.1007/s11004-015-9625-7>, 2016b.
- Metternicht, G. I., and Zinck, J. A.: Remote sensing of soil salinity: Potentials and constraints, Remote Sensing of Environment, 85, 1-20, [https://doi.org/10.1016/s0034-4257\(02\)00188-8](https://doi.org/10.1016/s0034-4257(02)00188-8), 2003.
- 25 Meyer, D., Dimitriadou, E., Hornik, K., Andreas, W., and Friedrich, L.: E1071: Misc functions of the department of statistics, probability theory group (formerly: E1071), tu wien, R package version 1.6-8, available at: <https://CRAN.R-project.org/package=e1071> (last access: 18 November 2018), 2017.
- Moeys, J.: Soiltexture: Functions for soil texture plot, classification and transformation, R package version 1.4.6, available at: <https://CRAN.R-project.org/package=soiltexture> (last access: 18 November 2018), 2018.
- 30 ~~Odeh, I. O. A., Todd, A. J., and Triantafyllis, J.: Spatial prediction of soil particle size fractions as compositional data, Soil Science, 168, 501-515, https://doi.org/10.1097/00010694_200307000_00005, 2003.~~
- Pahlavan-Rad, M. R., and Akbarimoghaddam, A.: Spatial variability of soil texture fractions and ph in a flood plain (case study from eastern iran), Catena, 160, 275-281, <https://doi.org/10.1016/j.catena.2017.10.002>, 2018.

- Poggio, L., and Gimona, A.: 3d mapping of soil texture in scotland, Geoderma Regional, 9, 5-16, <https://doi.org/10.1016/j.geodrs.2016.11.003>, 2017.
- R Core Team: R: A language and environment for statistical computing, R Foundation for Statistical Computing, Vienna, Austria. available at: <https://www.R-project.org/> (last access: 18 November 2018), 2018.
- 5 Saito, T., and Rehmsmeier, M.: Precrec: Fast and accurate precision-recall and roc curve calculations in r, Bioinformatics, 33, 145-147, <https://doi.org/10.1093/bioinformatics/btw570>, 2017.
- Salazar, E., Giraldo, R., and Porcu, E.: Spatial prediction for infinite-dimensional compositional data, Stochastic Environmental Research and Risk Assessment, 29, 1737-1749, <https://doi.org/10.1007/s00477-014-1010-4>, 2015.
- 10 Schliep, K., and Hechenbichler, K.: Kknn: Weighted k-nearest neighbors, R package version 1.3.1, available at: <https://CRAN.R-project.org/package=kknn> (last access: 18 November 2018), 2016.
- Song, X.-D., Brus, D. J., Liu, F., Li, D.-C., Zhao, Y.-G., Yang, J.-L., and Zhang, G.-L.: Mapping soil organic carbon content by geographically weighted regression: A case study in the heihe river basin, china, Geoderma, 261, 11-22, <https://doi.org/10.1016/j.geoderma.2015.06.024>, 2016.
- 15 Subasi, A.: Eeg signal classification using wavelet feature extraction and a mixture of expert model, Expert Systems with Applications, 32, 1084-1093, <https://doi.org/10.1016/j.eswa.2006.02.005>, 2007.
- ~~Sun, X. L., Wu, Y. J., Wang, H. L., Zhao, Y. G., and Zhang, G. L.: Mapping soil particle size fractions using compositional kriging, cokriging and additive log ratio cokriging in two case studies, Mathematical Geosciences, 46, 429-443, https://doi.org/10.1007/s11004-013-9512-z, 2014.~~
- 20 Taalab, K., Corstanje, R., Zawadzka, J., Mayr, T., Whelan, M. J., Hannam, J. A., and Creamer, R.: On the application of bayesian networks in digital soil mapping, Geoderma, 259, 134-148, <https://doi.org/10.1016/j.geoderma.2015.05.014>, 2015.
- Taghizadeh-Mehrjardi, R., Nabiollahi, K., Minasny, B., and Triantafilis, J.: Comparing data mining classifiers to predict spatial distribution of usda-family soil groups in baneh region, iran, Geoderma, 253, 67-77, <https://doi.org/10.1016/j.geoderma.2015.04.008>, 2015.
- 25 Thompson, J. A., Roecker, S., Grunwald, S., and Owens, P. R.: Chapter 21 - digital soil mapping: Interactions with and applications for hydropedology, in: Hydropedology, edited by: Lin, H., Academic Press, Boston, 665-709, 2012.
- ~~Tolosana-Delgado, R., Mueller, U., and van den Boogaart, K. G.: Geostatistics for Compositional Data: An Overview, Math Geosci., 51, 485-526, 10.1007/s11004-018-9769-3, 2019.~~
- 30 van den Boogaart, K. G., and Tolosana-Delgado, R.: "Compositions": A unified r package to analyze compositional data, Computers & Geosciences, 34, 320-338, <https://doi.org/10.1016/j.cageo.2006.11.017>, 2008.
- Vapnik, V.: The support vector method of function estimation, Nonlinear modeling: Advanced black-box techniques, edited by: Suykens, J. A. K., and Vandewalle, J., 55-85 pp., 1998.

- Walvoort, D. J. J., and de Gruijter, J. J.: Compositional kriging: A spatial interpolation method for compositional data, Mathematical Geology, 33, 951-966, <https://doi.org/10.1023/a:1012250107121>, 2001.
- Wang, Z., and Shi, W.: Mapping soil particle-size fractions: A comparison of compositional kriging and log-ratio kriging, Journal of Hydrology, 546, 526-541, <https://doi.org/10.1016/j.jhydrol.2017.01.029>, 2017.
- 5 Wang, Z., and Shi, W.: Robust variogram estimation combined with isometric log-ratio transformation for improved accuracy of soil particle-size fraction mapping, Geoderma, 324, 56-66, <https://doi.org/10.1016/j.geoderma.2018.03.007>, 2018.
- Wu, B., Yan, N., Xiong, J., Bastiaanssen, W. G. M., Zhu, W., and Stein, A.: Validation of etwatch using field measurements at diverse landscapes: A case study in hai basin of china, Journal of Hydrology, 436, 67-80,
- 10 <https://doi.org/10.1016/j.jhydrol.2012.02.043>, 2012.
- Wu, W., Li, A.-D., He, X.-H., Ma, R., Liu, H.-B., and Lv, J.-K.: A comparison of support vector machines, artificial neural network and classification tree for identifying soil texture classes in southwest china, Computers and Electronics in Agriculture, 144, 86-93, <https://doi.org/10.1016/j.compag.2017.11.037>, 2018.
- Yang, R.-M., Zhang, G.-L., Liu, F., Lu, Y.-Y., Yang, F., Yang, F., Yang, M., Zhao, Y.-G., and Li, D.-C.: Comparison of boosted regression tree and random forest models for mapping topsoil organic carbon concentration in an alpine ecosystem, Ecological Indicators, 60, 870-878, <https://doi.org/10.1016/j.ecolind.2015.08.036>, 2016.
- 15 Yi, C., Li, D., Zhang, G., Zhao, Y., Yang, J., Liu, F., and Song, X.: Criteria for partition of soil thickness and case studies, Acta Pedologica Sinica, 52, 220-227, 2015.
- Yoo, K., Amundson, R., Heimsath, A. M., and Dietrich, W. E.: Spatial patterns of soil organic carbon on hillslopes: Integrating geomorphic processes and the biological c cycle, Geoderma, 130, 47-65,
- 20 <https://doi.org/10.1016/j.geoderma.2005.01.008>, 2006.
- Zeraatpisheh, M., Ayoubi, S., Jafari, A., and Finke, P.: Comparing the efficiency of digital and conventional soil mapping to predict soil types in a semi-arid region in iran, Geomorphology, 285, 186-204, <https://doi.org/10.1016/j.geomorph.2017.02.015>, 2017.
- 25 Zeraatpisheh, M., Ayoubi, S., Jafari, A., Tajik, S., and Finke, P.: Digital mapping of soil properties using multiple machine learning in a semi-arid region, central iran, Geoderma, <https://doi.org/10.1016/j.geoderma.2018.09.006>, 2018.
- Zhang, S.-w., Shen, C.-y., Chen, X.-y., Ye, H.-c., Huang, Y.-f., and Lai, S.: Spatial interpolation of soil texture using compositional kriging and regression kriging with consideration of the characteristics of compositional data and environment variables, Journal of Integrative Agriculture, 12, 1673-1683, [https://doi.org/10.1016/s2095-3119\(13\)60395-0](https://doi.org/10.1016/s2095-3119(13)60395-0), 2013.
- 30 Zhang, X., Liu, H., Zhang, X., Yu, S., Dou, X., Xie, Y., and Wang, N.: Allocate soil individuals to soil classes with topsoil spectral characteristics and decision trees, Geoderma, 320, 12-22, https://doi.org/10.1016/j.geoderma.2018.01.023, 2018.

Zhao, Z., Chow, T. L., Rees, H. W., Yang, Q., Xing, Z., and Meng, F.-R.: Predict soil texture distributions using an artificial neural network model, Computers and Electronics in Agriculture, 65, 36-48,

<https://doi.org/10.1016/j.compag.2008.07.008>, 2009.

5 Zhu, A. X., Yang, L., Li, B., Qin, C., English, E., Burt, J. E., and Zhou, C.: Purposive Sampling for Digital Soil Mapping for Areas with Limited Data, In: Digital Soil Mapping with Limited Data, edited by: Hartemink, A. E., McBratney, A., and Mendonça-Santos, M. d. L., Springer Netherlands, Dordrecht, 233-245, 2008.